Materials Today Energy 44 (2024) 101643

Contents lists available at ScienceDirect

Materials Today Energy

journal homepage: www.journals.elsevier.com/materials-today-energy/

Bi_2Te_3-based flexible thermoelectrics

Mengran Chen [a], Zhendong Mao [a], Yuru Ji [a], Peng-an Zong [a, **], Qihao Zhang [b, *]

[a] College of Materials Science and Engineering, Nanjing Tech University, Nanjing 210009, China
[b] Light Technology Institute, Karlsruhe Institute of Technology, Engesserstrasse 13, 76131, Karlsruhe, Germany

ARTICLE INFO

Article history:
Received 30 April 2024
Received in revised form
28 June 2024
Accepted 29 June 2024
Available online 4 July 2024

Keywords:
Bi_2Te_3 films
Flexiblility
Thermoelectric performance
Deposition
Composite

ABSTRACT

Bi_2Te_3-based materials stand out as the top-performing material for thermoelectric applications at room temperature. However, its inherent rigidity has posed challenges for widespread usage in flexible thermoelectric conversion systems. Recent endeavors have focused on achieving Bi_2Te_3-based flexible films through bulk thinning, physical/chemical deposition, paste casting, as well as the template method. These efforts have led to a surge in research publications. This review aims to offer a comprehensive update on the synthesis approaches, microstructures, thermoelectric performances/flexibility, and the underlying mechanisms. Future research should focus on investigating innovative deposition techniques, exploring new composite phases/templates, refining fabrication parameters, and among others, to enhance the thermoelectric performances as well as flexibility.

1. Introduction

Flexible electronics, with the ability to withstand bending, rolling, folding, or stretching, have attracted considerable interest in academic and commercial circles. Nevertheless, these electronics still largely rely on conventional batteries as their primary power source, requiring frequent recharging and regular maintenance, leading to inconvenience and potential safety risks. Thus, there is a pressing need to develop a safe, maintenance-free, and flexible power source capable of powering flexible electronics. Thermoelectric (TE) materials present a promising avenue as they enable the direct conversion of heat into electricity, offering benefits such as being silent, pollution-free, and maintenance-free operation. The efficiency of TE materials is quantified through the dimensionless figure of merit, $zT = S^2\sigma T/\kappa$, wherein S denotes the Seebeck coefficient, σ represents the electrical conductivity, T signifies the absolute temperature, and κ denotes the thermal conductivity. The power factor (PF), $S^2\sigma$, serves as a comprehensive indicator of electrical properties. The κ comprises electronic thermal conductivity, κ_e and lattice thermal conductivity, κ_l [1–3]. Achieving a higher zT value necessitates materials with high σ and S values, as well as low κ. Nonetheless, these three parameters are mutually dependent, emphasizing the need for coordinated regulation to obtain zTs [4–8].

Although a plethora of newly discovered materials exhibiting exceptionally high zTs have surfaced, such as copper chalcogenides, tin selenide, among others, their real application needs further verification. High-temperature (>900 K) TE devices often employ SiGe alloys, with doping variations involving phosphorus or boron. Mid-temperature (500–900 K) TE materials typically include $CoSb_3$, PbTe, and similar compounds. The most commonly utilized room-temperature (RT) TE materials comprise Bi_2Te_3 alloys, specifically alloying Bi_2Te_3 with Sb_2Te_3 for p-type, and with Bi_2Se_3 for n-type compositions, respectively. The structural configuration of Bi_2Te_3, depicted in Fig. 1a, manifests a periodic layered structure where Bi–Te constituents establish interconnections through covalent/ionic bonding, while van der Waals (vdW) forces operate between successive Te atomic layers. Consequently, the TE properties of Bi_2Te_3-based materials demonstrate pronounced anisotropic traits. Bi_2Te_3 exhibits a narrow band gap of ~0.3 eV (Fig. 1b). The p-type and n-type variants of Bi_2Te_3 with remarkable RT zTs are usually used as p-type and n-type legs in TE devices, as shown in Fig. 1c.

Significant progress has been made in enhancing the zTs of bulk Bi_2Te_3-based materials (Fig. 1d). The zone-melting method offers precise control over the purification process, enabling the production of high-quality Bi_2Te_3-based materials with enhanced zTs. The thermal deformation process used in sample preparation

* Corresponding author.
** Corresponding author.
E-mail addresses: pazong@njtech.edu.cn (P.-a. Zong), qihao.zhang@kit.edu (Q. Zhang).

https://doi.org/10.1016/j.mtener.2024.101643

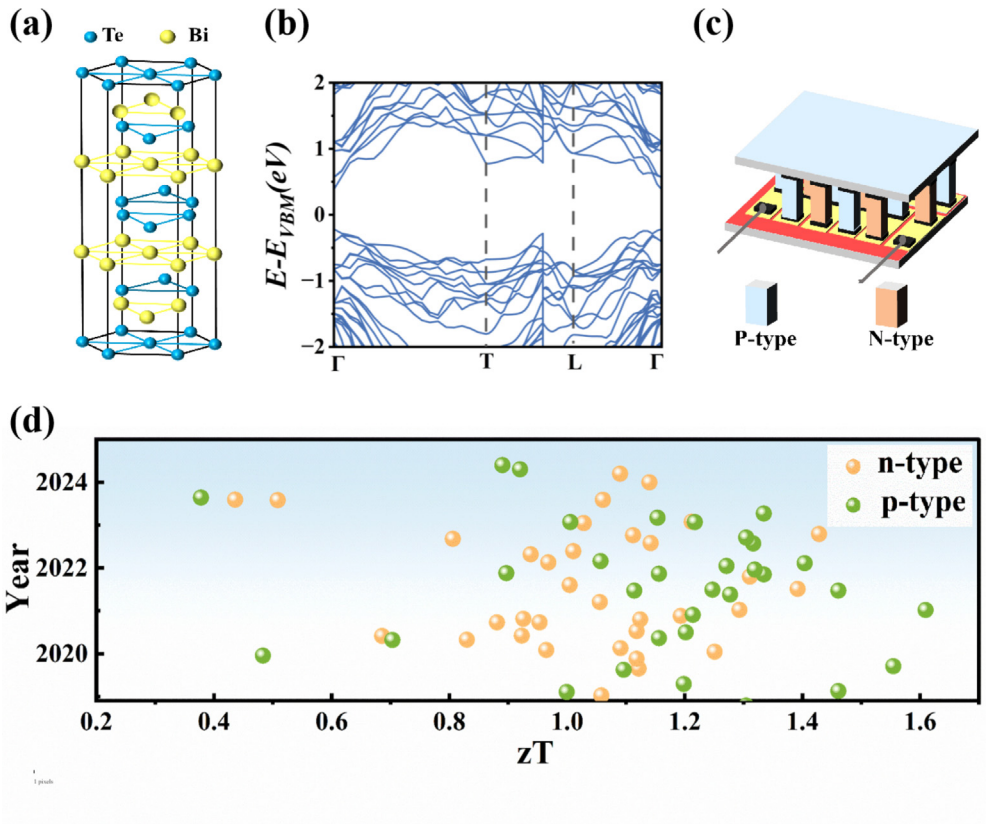

Fig. 1. Bi_2Te_3-based materials and device. (a) Schematic diagram of atomic structure. (b) Electronic structure [95]. Copyright 2023, Springer Nature. (c) TE device composed of n-type and p-type Bi_2Te_3-based legs. (d) The zT values of Bi_2Te_3-based materials reported since 2019 [9,17–81]. TE, thermoelectric.

may induce lattice distortions, dislocation formation, and nano-crystalline structures, consequently resulting in a notable decrease in the κ_l and thereby augmenting its zT. Notably, the p-type variant of Bi_2Te_3 can attain a zT of 1.6, whereas the n-type counterpart can achieve a zT value of 1.42 [9,62]. Advancements in microstructural engineering at the nanoscale have opened up new avenues for optimizing the zTs of Bi_2Te_3-based materials [10,11]. Grain boundary recrystallization and subnano regions have emerged as pivotal factors contributing to the attainment of high plateau zTs for Bi_2Te_3 nanoflakes. Bi_2Te_3 fabricated through the melt-spinning technique exhibits a ribbon-like nanophase structure, effectively reducing the κ_l and finally enhancing the zT [12,13]. Furthermore, the ball milling of Bi_2Te_3 ingots followed by sintering into nano-crystalline bulk materials yields exceptionally low κ_l values [14], with resultant p-type Bi_2Te_3 materials achieving a zT of 1.4 at 373 K [15]. Additionally, nanocompositing serves as another effective strategy for substantially decreasing κ_l, thereby further increasing the zT. Notably, the incorporation of $(Bi, Sb)_2Te_3$ with nano-SiC has been demonstrated to yield a zT of 1.33 at 373 K [16].

Although recent advancements have been made in enhancing the TE performance of bulk Bi_2Te_3-based materials, their intrinsic rigidity limits their application for flexible TE conversions [82,83]. The development of Bi_2Te_3-based flexible TE films and devices holds promise for applications requiring adherence to curved surfaces, such as human skin, facilitating the conversion of heat into electricity while minimizing heat loss during energy transfer [84–90]. Up to now, various methods have been employed in the fabrication of Bi_2Te_3-based flexible TE films, including bulk-thinning, physical or chemical deposition, paste casting, and the template method, among others [91,92]. The aim of this work is to offer an exhaustive comprehension of the synthesis, microstructure of Bi_2Te_3-based flexible films, as well as the performance optimization mechanisms (Fig. 2). Furthermore, the prospective challenges are delineated to stimulate ongoing research endeavors in this domain.

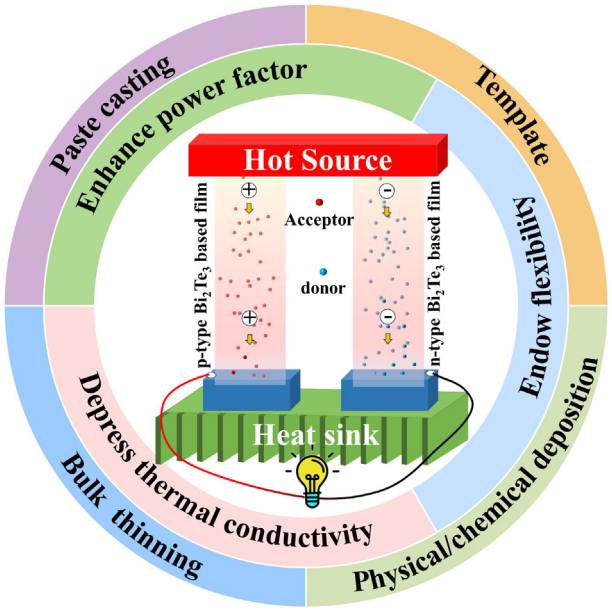

Fig. 2. Schematic outline of the review, including material fabrication and optimization of thermoelectric performance as well as flexibility.

2. Synthesis and microstructures of Bi_2Te_3-based flexible films

There are mainly four methods for preparing Bi_2Te_3-based flexible films: bulk thinning, physical/chemical deposition, paste casting, and template method. The uniqueness of the bulk thinning method lies in the fact that the film is exfoliated from a Bi_2Te_3-based single crystal. Although this method demonstrates superior TE performance, the film size is limited by the size of the single crystals, which are time-consuming and energy-intensive to grow. Additionally, manual exfoliation is inefficient, posing challenges for scaling up production. In contrast, films produced by physical/chemical deposition have lower TE performance compared to those produced by bulk thinning. However, this method offers much higher production efficiency due to rapid deposition, and the film size and composition are controllable. The limitation is the thickness, which is restricted to the nano to several micrometer range. Paste casting can produce much thicker films, but at the expense of TE performance due to the introduction of some guest phases with lower TE performance. The template method involves using conducting materials such as metal or carbon fiber networks as templates. This can compromise the *S* because of the high intrinsic carrier concentration (*n*) of the templates.

2.1. Bulk-thinning

Bulk-thinning is a process used to fabricate thin films directly from bulk materials. In this technique, a bulk material is mechanically thinned down to the desired thickness, usually ranging from nanometers to micrometers. Bulk-thinning offers advantages such as precise control over film thickness and high uniformity. It enables the creation of thin films with tailored properties [93,94]. As shown in Fig. 3a–c, researchers cut the prepared $Bi_{0.5}Sb_{1.5}Te_3$ (BST) and $Bi_2Te_{2.7}Se_{0.3}$ (BTS) single crystals (SC) in half along the (000*l*) faces of the single crystals, followed by fastening the transparent tape on the surface of the cut crystals [95]. Finally, the Bi_2Te_3 film was peeled off together with the tape to produce p-type and n-type Bi_2Te_3-based films. Staggered-layer structures, formed by atomic rearrangement around the vdW gap, were spontaneously generated during exfoliation. This staggered layer of Bi_2Te_3-based flexible films enhances stress propagation, leading to elastic bending while minimizing the attenuation of carrier transport along the thermal gradient. As shown in Fig. 3d and e, the atomic configurations of both the SC and the thin film composed of p-type BST along the [100] crystallographic zone axis were elucidated. As depicted in Fig. 3d, repetitive quintuple layers featuring a Te(1)–(BiSb)–Te(2)–(BiSb)–Te(1) sequence were discerned within the vdW gaps of the BST SC. In comparison, the BST film displayed an atomic structure with distinct staggered layers around the vdW gaps (Fig. 3e), where the lower two layers within the vdW gap progressively transformed into the upper two layers. Notably, the intensity of the Te atomic columns within the staggered layers exhibited a gradual increase, while the intensity of the BiSb columns displayed an inverse trend. These findings suggest a continual interchange between Te and BiSb layers, potentially attributed to atomic mobility within the vdW gaps. This distinctive structural configuration could induce a redistribution of strain around the vdW gaps, as evidenced by the corresponding strain mappings. The observed strain distribution delineates a greater fluctuation in film strain, potentially making it more resistant to deformation compared to the SC counterpart.

2.2. Physical/chemical deposition

Compared to bulk-thinning, physical/chemical deposition techniques, mainly magnetron sputtering, thermal evaporation,

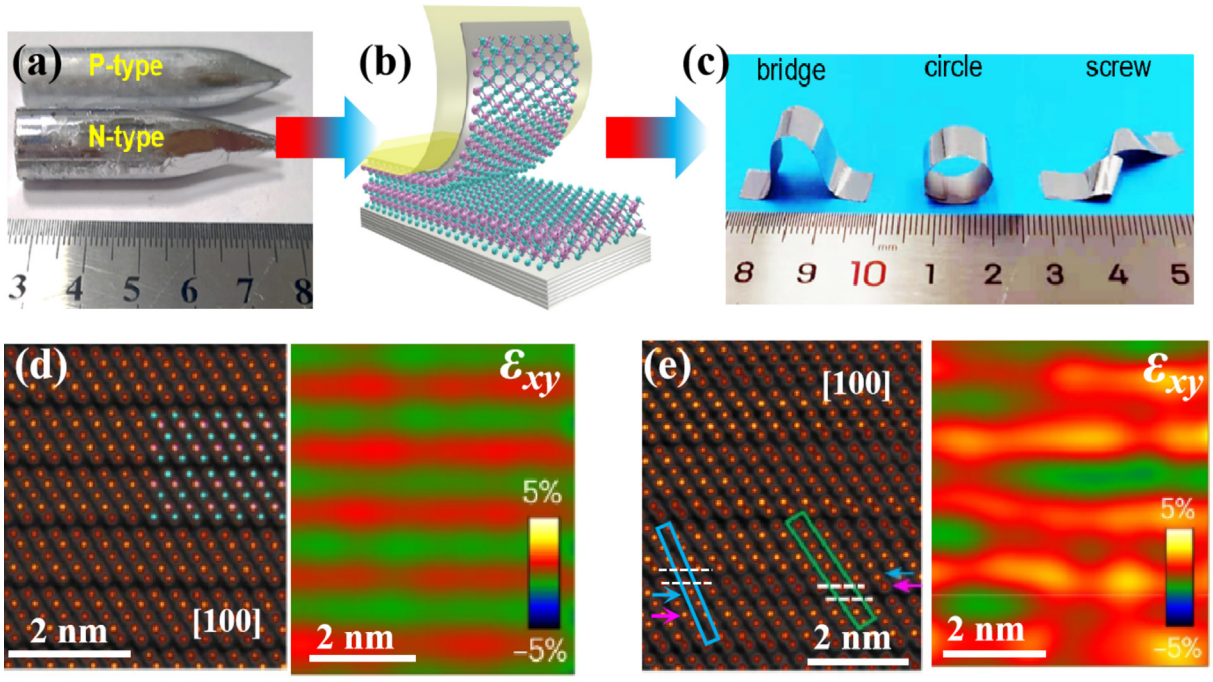

Fig. 3. Schematic depiction of the bulk-thinning process and microstructures of Bi_2Te_3-based flexible films. (a) p-type $Bi_{0.5}Sb_{1.5}Te_3$ and n-type $Bi_2Te_{2.7}Se_{0.3}$ single crystals. (b) Film extraction along the cleavage surface of the single crystal via adhesive tape. (c) Typical flexible films in different bending states. Atomic-resolution HAADF-STEM images with pseudocolor and corresponding strain maps of the p-type single crystal (d) and thin film (e), the inset in (d) revealing the BST crystal structure, with the BiSb and Te atomic columns labeled in orange and cyan, respectively. The dashed lines in (e) indicate the vdW gaps around the staggered layer. The blue and green boxes in (e) mark the atomic columns, while the blue and purple arrows point to the position of the staggered layer [95].

laser deposition, and electrodeposition offer significant advantages in terms of process complexity and film size. These techniques allow precise control over the composition and deposition rate. Additionally, they can create uniform thin films on complex geometries and large-area substrates [96,97]. For physical deposition, the presence of a substrate provides essential mechanical support for the Bi_2Te_3 matrix, ensuring their integrity and stability during deposition, subsequent processing, and application. Commonly used flexible substrates include polyimide (PI) films, polyethylene terephthalate (PET) [98], etc. Among them, PI stands out as the foremost thin-film insulating material, which exhibits extremely high thermal stability and is capable of long-term use at temperatures up to 678 K without decomposition [99]. However, the hydrophobic nature of PI requires surface modification to ensure the continuous deposition of Bi_2Te_3 matrix [100,101]. These methods include plasma irradiation, UV/ozone treatment, and acid or base treatments [102,103]. In the chemical deposition process, particularly electrodeposition, a conductive working electrode is essential. This electrode serves either as a platform for the deposition of Bi_2Te_3-based films, which can be subsequently transferred or as a template for forming a composite.

2.2.1. Magnetron sputtering

Magnetron sputtering is a highly effective technique employed for the deposition of Bi_2Te_3-based films [96,104]. In this process, a Bi_2Te_3-based target is bombarded with high-energy ions in a low-pressure environment. These ions dislodge atoms from the target surface, which then deposit onto a substrate [105]. This process offers several advantages. Firstly, it allows for precise control over the thickness and composition, ensuring uniformity and reproducibility. Additionally, it operates at relatively low temperatures. By adjusting parameters such as sputtering power, gas pressure, and substrate temperature, one can fine-tune the film structure and morphology. Therefore. magnetron sputtering facilitates the deposition of Bi_2Te_3-based films with tailored properties. However, magnetron sputtering does present certain drawbacks. These include elevated material costs, primarily attributed to the utilization of high-purity targets essential, stringent preparation conditions, including high vacuum levels, and elevated temperatures [106,107].

As shown in Fig. 4a, Nuthongkum et al. [104] prepared a flexible Bi_2Te_3 film on a PI substrate by radio frequency (RF) magnetron sputtering. They investigated the effect of sputtering pressure on the Te content and morphology of the films (Fig. 4b and c). At 0.8 Pa, the film revealed a smooth surface with a Te content lower than 50 at.%. When the sputtering pressure increased to 1.4 Pa, the Te content increased to 57 at.%; while larger particles and more distinct boundaries were formed, resulting in a rougher surface. When the pressure increased to 1.6 Pa, the Te content decreased to 54%; while grain agglomeration became more pronounced, and clear particle boundaries appeared. For the effect on Te content, when the sputtering pressure increases, the Ar^+ ions will be reduced to neutral Ar [108], which obstructs the Bi deposition, thereby increasing the Te content. Further increase in pressure will lead to obstruction of both Bi and Te deposition, thus decreasing Te content. For the effect on film morphology, the increase in sputtering pressure leads to a higher collision probability between sputtered particles and gas molecules, thereby reducing the mean free path of the sputtered particles. Particles with lower kinetic energy have insufficient mobility to effectively aggregate and grow, leading to coarse surface morphology [108–110].

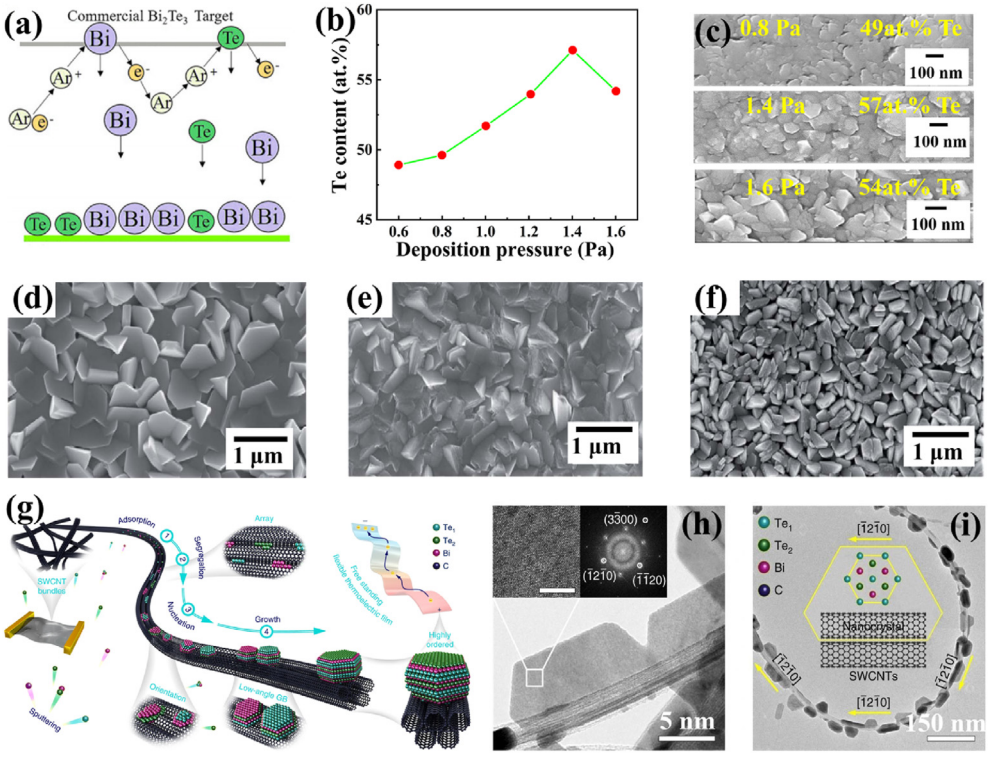

Fig. 4. Magnetron sputtering and microstructures of Bi_2Te_3-based films. (a) Schematic diagram of the formation of Bi_2Te_3 film by magnetron sputtering. (b) Gas pressure dependence of Te atomic percentage (at.%). (c) Surface SEM images at 0.8, 1.4, and 1.6 Pa Ar gas pressures [104]. Copyright 2017, Royal Society of Chemistry. Surface SEM images of $Bi_{0.5}Sb_{1.5}Te_3$ films deposited with modulated Te-target sputtering powers of 10 W (d), 20 W (e), and 30 W (f), respectively [107]. Copyright 2020, Royal Society of Chemistry. (g) Schematic diagram of the fabrication process of a freely suspended Bi_2Te_3-SWCNT hybrid by magnetron sputtering. (h) Adjacent Bi_2Te_3 nanocrystals firmly affixed onto a single SWCNT bundle. Inset: corresponding high-resolution image and FFT pattern. (i) Bi_2Te_3 nanocrystals positioned atop a curved SWCNT bundle. Inset presents an illustration detailing the alignment of Bi_2Te_3 with SWCNT orientation [106]. Copyright 2019, Springer Nature. SEM, scanning electron microscope; SWCNT, single-walled carbon nanotube.

The sputtering power can also affect the microstructures of the films, as reported by Shang et al. [107]. When the sputtering power of the Te target is 10 W (Fig. 4d), the in-plane size of $Bi_{0.5}Sb_{1.5}Te_3$ nanosheets was ~400 nm. Under an increasing sputtering power over 10 W, the size of $Bi_{0.5}Sb_{1.5}Te_3$ nanosheets was constantly decreased (Fig. 4e and f). Jin et al. prepared Bi_2Te_3/single-walled carbon nanotube (SWCNT) [106] and Bi_2Te_3/cellulose fibers (CFs) [111] composite films by magnetron sputtering. Typically, they present the fabrication process of flexible Bi_2Te_3/SWCNT materials by assembling layer-structured Bi_2Te_3 onto a carbon nanotube (CNT) scaffold, as depicted in Fig. 4g. The resulting flexible, free-standing thin-film TE material comprises highly ordered (000l)-textured Bi_2Te_3 nanocrystals firmly anchored on high-quality SWCNT bundles (Fig. 4h and i).

2.2.2. Thermal evaporation deposition

Thermal evaporation deposition involves heating Bi_2Te_3 in a vacuum chamber until it reaches its vaporization temperature. The vaporized atoms then travel in the vacuum and condense onto a substrate, forming a thin film [105,112,113]. Thermal evaporation excels in producing uniformly thick films across expansive areas, crucial for industrial-scale manufacturing. The vacuum environment significantly reduces contamination, ensuring the purity and consistency of the films. However, conventional thermal evaporation methods encounter challenges due to the disparate evaporation rates of Bi and Te from a single source, leading to notable compositional deviations from the desired.

It was revealed that the deposited films are Te-rich when the evaporation current (EVC) is lower than 100 A and become Bi-rich under higher current. Fan et al. [114] balanced the Bi and Te contents in Bi_2Te_3 films by a two-step thermal evaporation method. A Te-rich layer was first deposited on the PI substrate at an EVC below 100 A. Then, a Bi-rich layer was deposited at an EVC over 100 A. Finally, rapid heat treatment was used to treat the films under vacuum. The film composition of Bi_2Te_3 remained nearly the same under varied rapid heat treatment conditions. These results indicated the successful fabrication of the stoichiometric and highly uniform Bi_2Te_3 thin films. As shown in Fig. 5a, Zheng et al. [115] utilized thermal evaporation to deposit precursor layers of Bi/Sb and Te on PI substrates. The Bi/Sb and Te samples with PI substrates were placed together in a glovebox, and external heating was applied to one side of the Te sample. Te gradually diffused into the Bi/Sb film under temperature gradients and grew into $Bi_xSb_{2-x}Te_3$ thin films. Finally, $Bi_xSb_{2-x}Te_3$ films were synthesized on the substrate that previously contained the Bi/Sb film, while the other substrate that previously contained the Te film became blank due to complete Te diffusion. The cross-sectional scanning electron microscope (SEM) image (Fig. 5b) revealed a dense polycrystalline structure. The energy dispersive spectroscopy mappings of Bi, Sb, and Te, demonstrated a uniform distribution of all elements (Fig. 5c). This method was also used by Singh et al. [116] and produced uniform $Bi_{1.2}Sb_{0.5}In_{0.3}Te_3$ films.

2.2.3. Laser deposition

Laser powder bed fusion (LPBF), alternatively known as selective laser melting (SLM), primarily employing a high-energy laser beam to selectively melt thin layers of Bi_2Te_3-based powder, deposited in a pre-defined pattern, layer by layer. Upon solidification and subsequent cooling, these layers fuse together to produce Bi_2Te_3-based films. This innovative manufacturing process offers numerous advantages, including the ability to fabricate complex geometries with high precision and efficiency. By precisely controlling the laser energy and scanning path, LPBF enables the production of parts with tailored microstructures and mechanical properties, leading to enhanced performance and functionality [117,118]. As shown in Fig. 6a–d, Yuan et al. [119] prepared flexible Bi_2Te_3 thin films on a PI substrate using LPBF. The Bi_2Te_3 alloy powder was ultrasonically dispersed to obtain a smooth and well-dispersed slurry. Subsequently, it was coated onto a PI substrate and patterned by laser printing, directly adhering to the PI substrate. The rapid heating and

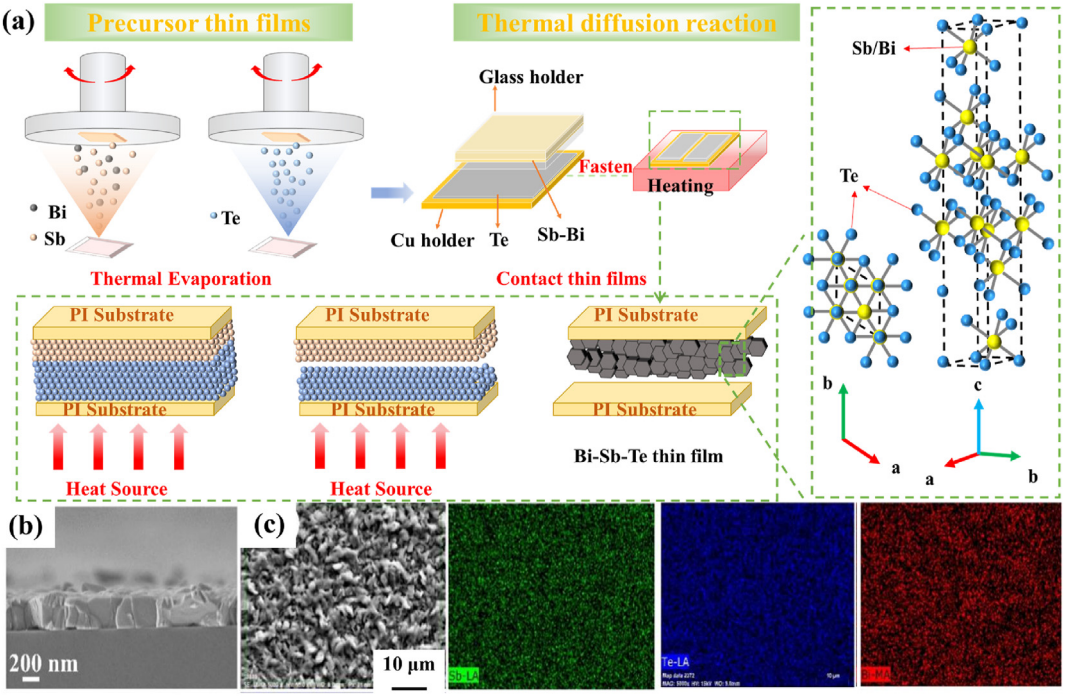

Fig. 5. Thermal-evaporation preparation and microstructures of Bi_2Te_3-based films. (a) Schematic illustration of the thermal-evaporation preparation process for the $Bi_xSb_{2-x}Te_3$ thin films. (b) Cross-sectional view, (c) surface view, and the element EDS mapping images [115]. Copyright 2024, Wiley. EDS, energy dispersive spectroscopy.

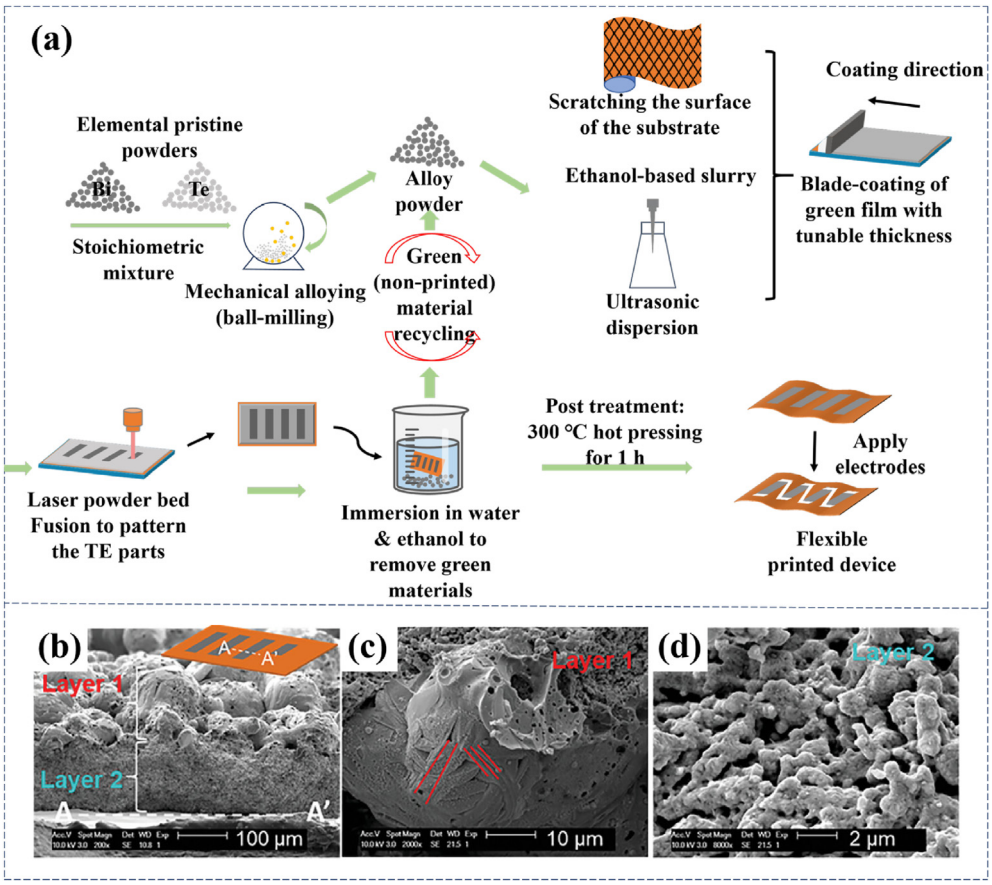

Fig. 6. Laser deposition and microstructures of Bi_2Te_3-based films. (a) Schematic diagram of the laser powder bed fusion method for the synthesis of Bi_2Te_3 films with patterns. (b) Cross-sectional SEM image. (c) Cross-sectional SEM of Layer 1. (d) Cross-sectional SEM of Layer 2 [119]. Copyright 2023, Wiley-Blackwell. SEM, scanning electron microscope.

cooling rates of laser printing also resulted in a film morphology with two distinct layers (Fig. 6b). As shown in Fig. 6c, the cross-section SEM revealed a unique bilayer structure. The top layer, Layer 1, enlarged from Fig. 6b, exhibited a typical spherical morphology, which was denser than the bottom layer. The bottom layer, Layer 2, showed a highly porous sintered powder-like morphology (Fig. 6d).

2.2.4. Electrodeposition

Electrodeposition is the process of depositing thin films onto a substrate surface through an electrochemical reaction. For the electrodeposition of Bi_2Te_3-based thin films, this technique involves passing an electric current through an electrolyte containing ions of Bi and Te, which causes these ions to migrate and adhere to the substrate surface, forming a thin film. The advantages of this technology include precise control over film thickness and composition, uniform deposition distribution, and the unique ability to deposit films onto complex-shaped substrates. Since electrodeposition requires conductive electrodes, it is necessary to transfer the electrodeposited Bi_2Te_3 film to an adhesive substrate for TE performance testing [120]. The electrodeposition process also has the advantages of fast deposition speed, low cost, and simple operation, thus it is competitive among the fabrication methods of Bi_2Te_3-based thin films. The three-electrode setup for electrodeposition of Bi_2Te_3 is shown in Fig. 7a. In this setup, one loop consists of the working electrode (WE), counter electrode (CE), and a power supply, while the other loop consists of the WE and a reference electrode (RE) to monitor the electrochemical reaction process. When an external voltage is applied, the WE becomes filled with electrons, establishing an electric field between the WE and the CE. This electric field causes the migration of Bi(III) and Te(IV) cations in the electrolyte toward the surface of the WE. These cations are then reduced on the surface of the WE, contributing to the deposition of Bi_2Te_3.

As depicted in Fig. 7b, the initial electrodeposition of Bi_2Te_3 was conducted utilizing potentiostatic or galvanostatic modes, wherein the applied potential or current density remains constant throughout the process. Nonetheless, the persistent deposition procedure fails to mitigate the detrimental impact of concentration polarization, thereby resulting in the formation of diminutive grain sizes, diverse orientations (Fig. 7c), and deviating compositions. Optimally, the fabrication of Bi_2Te_3 thin films employs pulse-mode deposition. This technique encompasses two distinct phases: during the "t_{on}" period, Bi(III) and Te(IV) ions undergo reduction and deposition onto the WE while the current is activated. Consequently, there is a rapid decrease in ionic concentration within the interfacial layer, leading to an increase in polarization. Subsequently, in the "t_{off}" phase, when the current is deactivated, ions within the electrolyte are propelled by chemical potential and diffuse into the interfacial layer to compensate, thereby mitigating concentration polarization (Fig. 7d and e) and facilitating the attainment of a dense structural configuration. Na et al. [120] prepared an n-type Bi_2Te_3 thin film by electrodeposition and then transferred it to a flexible substrate. The surface morphology and crystallinity of electrodeposited Bi_2Te_3 films depend on the deposition potential, V_{dep}. The surface morphology of Bi_2Te_3 films deposited by applying negative V_{dep} is rough with some large grains observed, and the distribution of grain sizes is not uniform

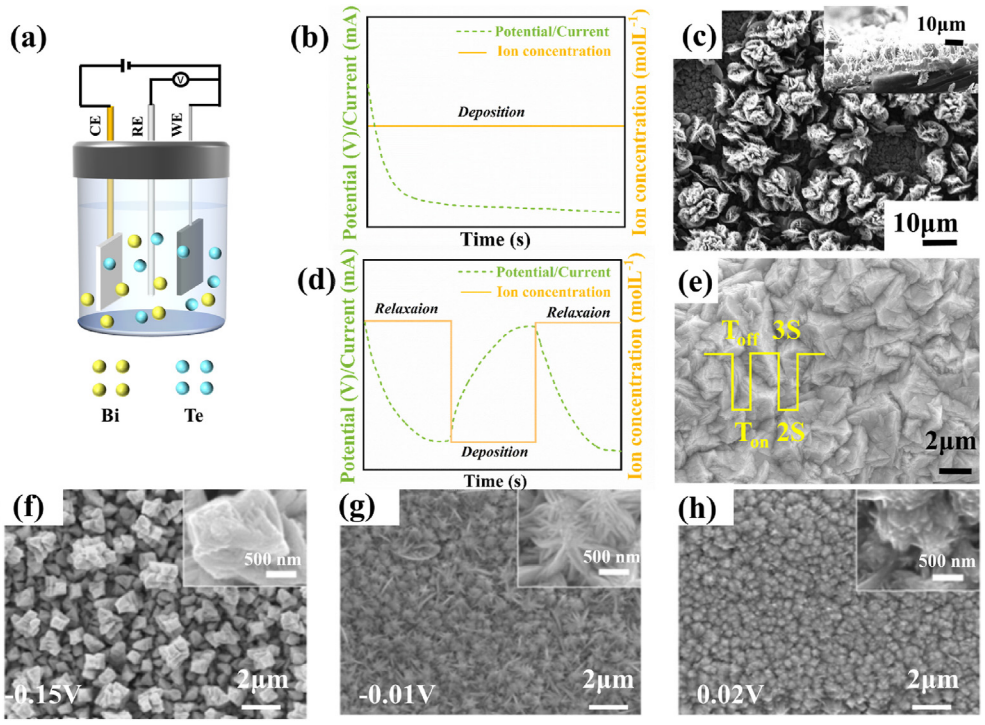

Fig. 7. Electrodeposition and microstructures of Bi_2Te_3-based films. (a) Schematic diagram of the deposition setup. Time dependencies of working potential/current and ion concentration (solid line) within the interfacial layer on WE in potentiostatic/galvanostatic mode (b) and two-step pulse mode (d). SEM images of the Bi_2Te_3 films by potentiostatic (c) and (e) pulse modes. SEM image of the Bi_2Te_3 film at potentials of (f) −0.15, (g) −0.01, (h) 0.02 V on a stainless steel substrate [120]. Copyright 2016, American Chemical Society. WE, working electrode; SEM, scanning electron microscope.

(Fig. 7f). However, the Bi_2Te_3 film deposited at −0.01 V showed a smaller grain size (Fig. 7g). When V_{dep} is shifted to a positive potential, the films exhibit highly dense and well-connected morphologies. And the films deposited under positive potential have small grain size and low roughness (Fig. 7h).

2.3. Paste casting

The paste-casting fabrication of Bi_2Te_3-based flexible films typically begins with the synthesis of the Bi_2Te_3-based paste, followed by solidification for film formation. Common methods for preparing Bi_2Te_3 paste entail physical mixing and the solvothermal method. Each method offers distinct advantages.

2.3.1. Paste synthesis

The physical mixing method involves directly stirring and mixing Bi_2Te_3-based powder with organics to create paste, which is then allowed to solidify to form a film. Song et al. [121] prepared the Bi_2Te_3/Poly(3,4-ethylenedioxythiophene):poly(styrenesulfonate) (PEDOT:PSS) paste by physical mixing. It was found that the dispersion state of the Bi_2Te_3 particles determines the film roughness. Zhang et al. [122] introduced polyvinyl alcohol (PVA) and $Bi_{0.5}Sb_{1.5}Te_3$ into PEDOT:PSS solution to obtain PEDOT: PSS/PVA/$Bi_{0.5}Sb_{1.5}Te_3$ paste before casting. The solvothermal method is commonly used for in-situ growth of Bi_2Te_3 matrix in paste synthesis. It provides a closed pressurized reaction system for the chemical reaction of precursor reactants in an organic solvent at a certain temperature to generate products. The closed system could help to promote the dissolution, diffusion, and transformation of the reactants, thereby improving the dispersibility, crystallinity, and yield of products. The method is cost-effective due to the low reaction temperature, short duration, and high yield [123,124]. Chen et al. [125] prepared the Bi_2Te_3/SWCNTs paste by the solvothermal method. Inorganic Bi_2Te_3 particles and nanosheets were successfully grown in situ on SWCNTs. As shown in Fig. 8a, Mao also prepared the Bi_2Te_3/graphene paste by a solvothermal method [126]. Due to the easy nucleation supported by graphene nanosheets, Bi_2Te_3 nanosheets grew within and on the graphene layer, as shown in Fig. 8b.

2.3.2. Film casting

Methods commonly employed for film formation after paste synthesis include vacuum filtration, printing, etc. Vacuum filtration relies on the pressure difference created by applying a vacuum to draw the liquid part from the paste through a porous filter membrane. As the liquid passes through the filter, the Bi_2Te_3-based materials are left behind, forming a thin film on the surface of the filter. Once dried, the thin film can be carefully peeled off from the filter membrane and collected. Zhao et al. [127] incorporated a small quantity of cellulose nanofibers (CNF) into Bi_2Te_3 powder, then utilized vacuum filtration to prepare a flexible CNF/Bi_2Te_3 film. In this composite, Bi_2Te_3 was evenly dispersed within the three-dimensional CNF network.

Printing techniques, including hand printing and screen printing, are commonly employed for the casting of Bi_2Te_3-based paste. Hand printing is a manual technique where the Bi_2Te_3-based paste is spread onto the substrate using a blade. After casting, the film is allowed to dry, either at RT or using controlled heating, to remove the solvent and bind the particles together. Hand printing offers simplicity and flexibility, allowing for the casting of Bi_2Te_3 paste onto various substrate shapes and sizes. It is suitable for small-scale production and prototyping. Cho et al. [128] prepared edge-oxide graphene-dispersed p-type $Bi_{0.4}Sb_{1.6}Te_3$ (EOG/BST) thin films by hand-printing. As shown in Fig. 8c, the EOG connected the individual BST grains well (Fig. 8d). Screen printing is a widely used technique for casting thick Bi_2Te_3 films. It involves pushing the

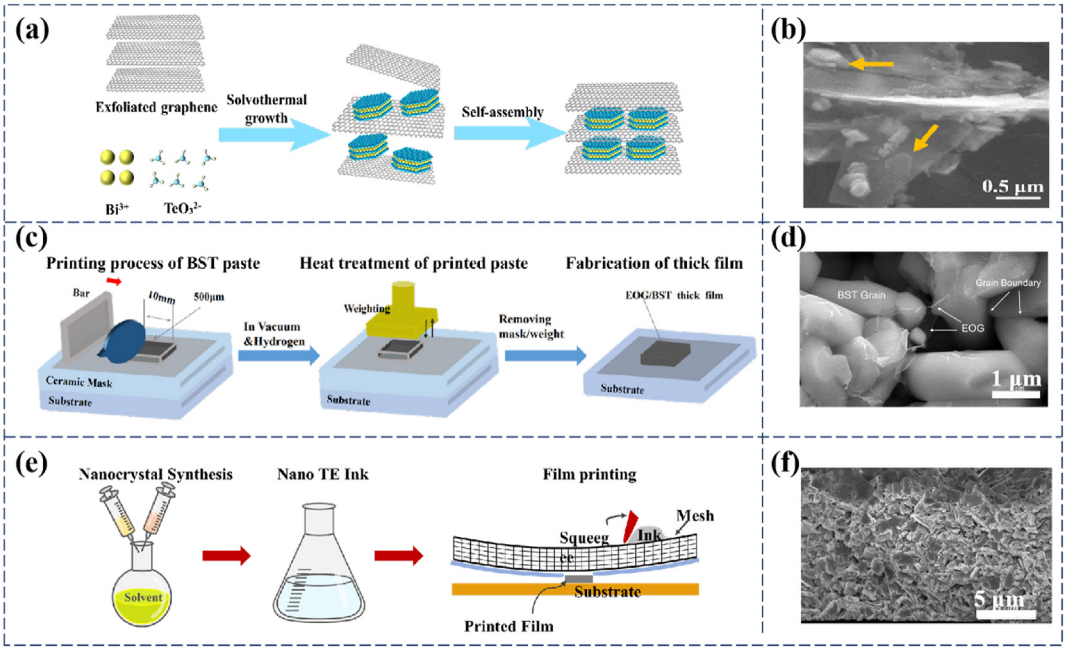

Fig. 8. Paste-casting and microstructures of Bi_2Te_3-based films. (a) In-situ synthesis of graphene/Bi_2Te_3 film by intercalating Bi_2Te_3 nanoplates into graphene nanosheets and (b) the microstructure. Copyright 2022, Wiley. Fabrication process of EOG/BST thick film by hand printing (c) and the microstructure (d). Copyright 2019, Elsevier. Screen-printing of $Bi_2Te_{2.8}Se_{0.2}$ films (e) and the microstructure (f) Copyright 2016, Springer Nature. EOG/BST, edge-oxide graphene-dispersed p-type $Bi_{0.4}Sb_{1.6Te3.}$

paste through a mesh screen onto the substrate surface. After casting, the substrate is dried to remove the solvent, and the paste is often cured at elevated temperatures to improve adhesion and conductivity. Screen printing allows for high throughput and precise control over the pattern. It is suitable for large-scale production of Bi_2Te_3-based thick films and complex device architectures. Varghese et al. [129] fabricated $Bi_2Te_{2.8}Se_{0.2}$ thin films using screen printing (Fig. 8e). The disadvantage of the screen printing method is that the prepared films often have edge defects and are of low density (Fig. 8f).

2.4. Template method

The template method leverages template-assisted fabrication techniques to synthesize monodisperse Bi_2Te_3-based nanofillers within a continuous polymer matrix or to grow Bi_2Te_3 within a three-dimensional template framework, such as conducting foams or woven carbon fibers. The template method capitalizes on the use of templates, which can be porous substrates or pre-designed structures, to guide the growth of Bi_2Te_3-based nanofillers or structures. By controlling the morphology and dimensions of the templates, precise control over the size, shape, and arrangement of the resulting Bi_2Te_3-based nanostructures can be achieved.

As shown in Fig. 9a, Wang et al. [130] prepared a Bi_2Te_3/PEDOT hybrid film by using an improved template method. Specifically, the Bi_2Te_3 nanophase was patterned by using a polystyrene nanosphere monolayer as a mask, combined with a vapor-phase polymerization process to synthesize the Bi_2Te_3/PEDOT hybrid film. Nanosphere lithography has been proven to be an effective approach to large-area periodic arrays of nanostructures on flexible substrates. It also has the advantages of good repeatability and controllable structural parameters [131–135]. As shown in Fig. 9b, monodisperse and periodic Bi_2Te_3 nanophases can be clearly observed in the PEDOT/Bi_2Te_3 hybrid films, which greatly reduce the κ and endow the films with flexibility. However, the cost of this template method is also relatively high. Shi et al. [136] deposited Bi_2Te_3 nanosheets on/inside nickel foam (NiFoam) template (Fig. 9c). The three-dimensional through-holes of the NiFoam were completely filled with Bi_2Te_3 nanoplates, and the nickel skeleton was also completely covered, as shown in Fig. 9d. Shi et al. [137] also prepared Bi_2Te_3/carbon fiber fabric (CFF) films with CFF as the template, as shown in Fig. 9e. The pretreated CFF consisted of numerous carbon fibers (CFs) with a diameter of ~10 μm, arranged in a crisscross pattern along both the warp and weft directions, intertwining at their intersections. The surface of the CFs became fully coated with Bi_2Te_3 after electrodeposition, exhibiting a finely needle-like morphology (Fig. 9f).

Among all methods used, the Bi_2Te_3/organics paste-casting is the most promising for scale-up and cost-down fabrication of flexible thick films, although it may encounter challenges in achieving complete dispersion of Bi_2Te_3-based nano/microparticles within a polymer matrix. One primary obstacle lies in the poor wettability between polymers and Bi_2Te_3-based particles, which can impede their uniform distribution. Additionally, the surface of Bi_2Te_3-based particles is prone to oxidation, further complicating their dispersion within the organic polymer matrix. These factors collectively contribute to the difficulty in achieving optimal dispersion and integration of Bi_2Te_3-based particles in such matrices [138,139].

3. Performance of the Bi_2Te_3-based films

The synthesis of Bi_2Te_3-based flexible films employs various techniques, each providing distinct benefits regarding film uniformity, compositional and microstructural control, and TE performance. The following sections will offer a detailed discussion of the TE performance of Bi_2Te_3-based films, analyzing the impact of the different fabrication methods.

3.1. Thermoelectric performance of bulk-thinning films

The TE performance of Bi_2Te_3-based flexible films prepared by bulk-thinning is the highest among all reported values (Table 1). Lu et al. [95] reported bulk-thinning fabrication of Bi_2Te_3-based films

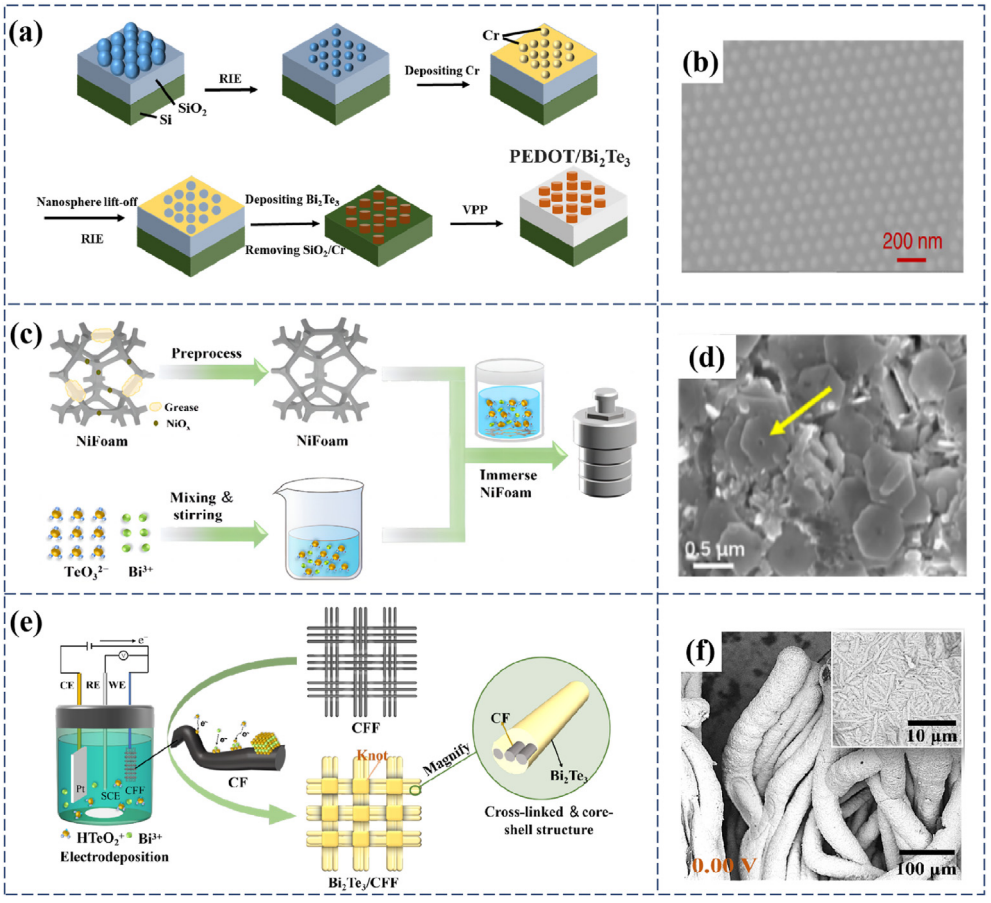

Fig. 9. Template method fabrication and microstructures of Bi_2Te_3-based films. (a) Schematic diagram of Bi_2Te_3/PEDOT composite film prepared by the template method and (b) the microstructure [130]. Copyright 2018, Springer Nature. (c) Schematic diagram of the synthesis of NiFoam/Bi_2Te_3 composite film by the template method and (d) the microstructure [136]. Copyright 2022, Multidisciplinary Digital Publishing Institute. (e) Schematic diagram of the synthesis of Bi_2Te_3/carbon fiber fabric by template method and (f) the microstructure [137]. Copyright 2022, Elsevier.

Table 1
TE properties and flexibility of Bi_2Te_3 based films at RT.

Materials	Methods	n	μ	σ	S	PF	κ	zT	fFOM	Ref.
$Bi_{0.5}Sb_{1.5}Te_3$	BT	~7	~130	~22.6	1.34	42.1	1.35	0.9	1.5×10^{-3}	[95]
$Bi_2Te_{2.7}Se_{0.3}$	BT	~4.5	~70	9.9	−2.2	45.7	1.22	1.1	1.5×10^{-3}	[95]
Bi_2Te_3	MS	62.6	6.7	6.7	−1.2	9.5	–	–	–	[104]
Bi_2Te_3	MS	9.3	57.4	6.9	−1.8	21.7	–	–	–	[110]
Bi_2Te_3/SWCNTs	MS	–	–	~5.3	−1.7	~16	0.53	0.89	7.5×10^{-5}	[106]
Bi_2Te_3/SWCNTs	MS	–	39.5	1.2	~−1.5	2.7	0.34	0.23	6.3×10^{-5}	[177]
Bi_2Te_3	TEP	141	2.2	5	−0.1	5.3	–	–	–	[142]
$Bi_{0.3}Sb_{1.7}Te_3$	TEP	–	–	~10	1.6	26.9	~0.8	0.98	–	[115]
Bi_2Te_3	TEP	4.8	34.7	2.8	−1.3	4.4	0.26	0.51	2×10^{-5}	[114]
Bi_2Te_3	ED	–	–	8.5	−1.3	1.5	–	–	–	[120]
Bi_2Te_3/SWCNTs	ST	–	–	2.4	0.4	0.3	–	–	1.3×10^{-3}	[125]
Bi_2Te_3/graphene	ST	~8	~17	1.5	0.4	0.2	1.9	3×10^{-3}	1.5×10^{-2}	[126]
Bi_2Te_3/rGO	VF	–	–	0.5	−1.5	1.1	~9.7	3.3×10^{-3}	–	[158]
Bi_2Te_3/rGO	PT	1.21	103.3	2	−12.7	3.2	0.47	0.2	1×10^{-2}	[159]
$Bi_{0.4}Sb_{1.6}Te_3$/EOG	PT	1.5	133	23.4	2.5	20.6	–	–	–	[128]
$Bi_2Te_{2.7}Se_{0.3}$/EOG	PT	~1.6	96.4	2.6	−2.4	15.4	–	–	–	[160]
Bi_2Te_3/PEDOT:PSS	PM	–	–	4.2	47.5	0.1	7×10^{-2}	0.04	–	[121]
$Bi_2Se_{0.3}Te_{2.7}$/CNF	PM	–	–	5.3	1.3	8.9	–	–	2.5×10^{-2}	[127]
$Bi_2Te_{3-x}Se_x$/CC	TP	–	–	4.4	−1.4	8.3	–	–	3.3×10^{-2}	[176]
Bi_2Te_3/NiFoam	TP	–	–	110.8	0.2	8.5			1.6×10^{-2}	[136]
Bi_2Te_3/CFF	TP	~11.3	~11.5	~2.8	−0.3	0.3	–	–	2.2×10^{-2}	[137]
Bi_2Te_3/PEDOT	TP	–	–	~4.4	−1.8	13.5	0.69	0.58	–	[130]

Note: Preparation methods are abbreviated: bulk-thinning (BT); physical deposition: magnetron sputtering (MS), thermal evaporation (TEP). chemical deposition: Electrodeposition (ED). paste casting: physical mixing (PM), solvothermal (ST), vacuum filtration (VF), printing (PT). template method (TP), thermoelectric (TE), room-temperature (RT). Units: n: 10^{19} cm^{-3}; μ: $cm^2/V/s$; σ: 10^2 S/cm; S: 10^2 V/K; PF: 10^2 μW/m/K^2; κ: W/m/K.

with a misfit layered structure. The RT *PF* reached 4.2 (p-type) and 4.6 (n-type) mW/m/K^2, exhibiting TE performance comparable to that of single crystals (SCs), and possessing good flexibility. This is mainly attributed to the interlocking layered structure, which not only promotes stress propagation but also maintains ultra-high conductivity. Flexible TE devices prepared from these films exhibited a high power density of up to 321 W/m^2 ($\Delta T = 60$ K), which is about an order of magnitude higher than that of traditional flexible devices. The bulk-thinning method can preserve the original structure to the greatest extent, thereby maintaining the excellent TE performance of the bulk Bi_2Te_3 material.

3.2. Thermoelectric performance of deposited/paste-casted films

Deposited or paste-casted films offer advantages in process flexibility, material utilization, and structural controllability. However, their TE performance is somewhat inferior to that of bulk-thinned films due to a high density of defects, which significantly deteriorates electrical transport. The performance variation among deposited or paste-casted films depends on specific processing parameters that influence their composition and microstructures.

3.2.1. Physical/chemical deposited Bi_2Te_3-based films

Nuthongkum et al. [104] reported that the *PF* first rose from 189 μW/cm/K^2–949 μW/cm/K^2, and then dropped to 190 μW/cm/K^2, due to the up and down of Te content, arising from the increasing deposition pressure. Kong et al. [110] achieved a high *PF* of 2167 μW/cm/K^2, which was due to the excellent (00l) film orientation at an optimal pressure. This was also confirmed by Somdock et al. [140]. The highly ordered crystal orientation reduced the density of grain boundaries and defects, thereby weakening carrier scattering and enhancing the μ. Annealing can smoothen the sputtered film, as reported by Kuang et al. [141]. The maximum *PF* value of the p-type BST and n-type BTS films were 430 μW/m/K^2 and 1230 μW/m/K^2, respectively.

Zheng et al. [142] reported an σ of 500.2 S/cm, and low *S* of 11.3 μV/K, due to poor crystallinity of Bi_2Te_3. The *PF* reached a maximum of 530 μW/m/K^2 after annealing due to increased crystallinity. By alloying with Bi, the *n* was optimized, achieving a *S* of 25 μW/K, leading to a maximum *PF* of 2690 μW/m/K^2 for $Bi_{0.3}Sb_{1.7}Te_3$ films [115]. The flexible Bi_2Te_3 thin films deposited by LPBF revealed a thickness of ~65 μm, a *PF* over 1500 μW/m/K^2, and a zT value of 0.25. The electrodeposited n-type Bi_2Te_3 films [120] grew along the (110) crystal direction, exhibiting higher crystallinity, leading to an σ of 691 S/cm and a maximum *PF* of 1473 μW/m/K^2.

3.2.2. Paste casted Bi_2Te_3-based films

The Bi_2Te_3-based flexible films prepared by the paste-casting method are usually composites with carbon, such as CNTs, graphene, reduced graphene oxide (rGO), or polymer materials as secondary phases. Although the secondary phases showed good flexibility, one or more values of their κ, *S*, and σ are not ideal for a high zT, lowering overall TE performance compared to films prepared by bulk-thinning or physical/chemical deposition methods. However, the paste-casting method allows for the production of relatively thick films, providing a degree of practical utility.

3.2.2.1. Carbon/Bi_2Te_3-based composite films. CNT/Bi_2Te_3-based composite films: CNTs exhibit significant promise as flexible TE materials owing to their nanoporous structure, unique electrical, coupled with exceptional flexibility [143,144]. For instance, Macleod et al. [145] reported single-walled SWCNTs with a peak *PF* of 700 μW/m/K^2. Incorporating CNTs into matrix ceramics has been proven effective in elevating σ while reducing κ [146], due to enhanced phonon scattering at the CNT/matrix interface.

Graphene/Bi_2Te_3-based composite films: graphene has attracted great interest since its discovery [147], because of its excellent mechanical and electrical properties. Due to the instability of the structure, many ripples with lengths of several nanometers to tens of nanometers usually appear on graphene surfaces [148]. Therefore, it is easy to wrap other particles nearby to keep themselves stable. The in-plane electron μ of graphene at RT reaches 2.5×10^5 cm^2/V/s, and its σ is 1×10^6 S/m, about 1.5 times that of copper, which is far beyond those of conventional metallic and semiconducting materials [149–153]. Thus, it can provide a fast carrier transport channel for Bi_2Te_3-based films [126,154–157].

rGO/Bi_2Te_3-based composite films: rGO is reduced from graphene oxide (GO). It can be a semiconductor or a conductor, depending on its reduction degree. GO is an insulator but possesses good dispersivity in an aqueous solution. Therefore, GO can be used as the precursor for rGO, and achieving good dispersivity before reduction. However, rGO still has a low σ, restricting the *PF* of the rGO/Bi_2Te_3 films [158,159]. EOG is a special type of rGO, which has oxidation groups only on edges, and thus its σ is higher than rGO. The enhanced σ is anticipated to significantly improve the TE properties of the composite film [160]. The p-type EOG/$Bi_{0.4}Sb_{1.6}Te_3$ TE film [128] achieved a maximum *PF* of 2060 μW/m/K^2, which was increased by 1.7 times.

3.2.2.2. Organic/Bi_2Te_3-based composite films. Conductive polymers inherently exhibit low κ, while Bi_2Te_3 boasts relatively good *PF*. Thus, their combination holds promise for achieving optimized comprehensive TE performance [161]. Currently, Poly(3,4-ethylenedioxythiophene):poly(styrenesulfonate) (PEDOT:PSS) [162,163] stand out as the most commonly utilized conductive polymers. These organic molecules not only contribute to the enhancement of TE properties but also confer increased flexibility to Bi_2Te_3-based films.

PEDOT:PSS aqueous solution comprising a high-molecular-weight polymer renowned for its remarkable conductivity. Consisting of two constituents, PEDOT and PSS, PEDOT:PSS is a synergistic blend where PEDOT, inherently insoluble in most solvents, becomes well-dispersed in aqueous solvents when emulsified with PSS. Within this composite, PEDOT assumes the role of charge conduction, while PSS acts as an insulator [164,165]. The flexible PEDOT:PSS/Bi_2Te_3 films combine PEDOT:PSS with different contents of Bi_2Te_3 [121] revealed *S* values fluctuating slightly within a range of 14.2 μV/K to 18.6 μV/K. The maximum σ reached 421 S/cm, corresponding to the highest *PF* of 9.9 μW/m/K^2. The flexible PEDOT:PSS/PVA/$Bi_{0.5}Sb_{1.5}Te_3$ films revealed a *PF* of 47.7 μW/m/K^2 and a zT value of 0.05 at 300 K [122].

Cellulose, though insulating, is one of the most abundant and renewable natural polymer materials [166]. Bacterial cellulose (BC), as a distinct cellulose variant, emerges as an eco-friendly biomaterial composed of CNF [167]. The attributes of BC include high porosity, exceptional tensile strength, and superb biocompatibility, making it a prime candidate for employment in a spectrum of flexible electronic devices [168–171]. The flexible CNF/$Bi_{0.5}Sb_{1.5}Te_3$ film [127] revealed an σ of 532 S/cm, *S* of 130 μV/K, leading to a *PF* of 889 μW/m/K^2.

3.3. Thermoelectric performance of template based films

The flexibility of Bi_2Te_3-based films can be optimized by introducing suitable templates, usually at the sacrifice of some TE performance. Flexible carbon cloth (CC) usually serves as a prevalent electrode material for electrochemical reactions owing to its low resistance and flexibility. Consequently, flexible conductive CC can

serve as the template for Bi_2Te_3-based material deposition, making it well-suited for integration into TE generators [172–175]. Kim et al. [176] synthesized $Bi_2Te_{3-x}Se_x$/CC films by utilizing flexible conductive CC as a substrate, achieving a maximum *PF* of 1300 μW/m/K^2 at 473 K. The CC facilitated an electrical pathway through the one-dimensional wire, thereby augmenting the σ. Shi et al. [137] reported that the *PF* of the annealed Bi_2Te_3/CFF film reached a peak value of 33.4 μW/m/K^2, a 300-fold increase compared to the pure CFF film. This enhancement stems from the formation of a cross-linked core-shell structure, which significantly enhanced the μ. Furthermore, the *S* of Bi_2Te_3/CFF was bolstered compared to CFF due to the decrease in *n*, resulting in a nearly two-order-of-magnitude improvement in the final *PF*. Moreover, Shi et al. [136] deposited Bi_2Te_3 nanosheets into porous NiFoam, followed by pressing and annealing to obtain a NiFoam/Bi_2Te_3 composite film with a porous filling structure. At RT, its *PF* is 850 μW/m/K^2 due to a variety of mechanisms. Wang et al. [130] devised a Bi_2Te_3/PEDOT hybrid film via the template method, yielding a zT value of ~0.58 at RT.

3.4. Flexibility of the Bi_2Te_3-based films

As universally recognized, when brittle materials such as glass and ceramics are reduced to thin dimensions, they exhibit enhanced flexibility. Specifically, crystalline silicon, traditionally rigid in nature, finds extensive application in wearable electronics as a foundational material for silicon microelectronics. This phenomenon occurs notably when the thickness diminishes to around 100 nm, making the material flexible [178]. Similarly, indium gallium zinc oxide, despite being an inherently rigid inorganic oxide, assumes flexibility when sufficiently thin, thus serving as a viable material for flexible transistors [179]. Therefore, the assessment of flexibility necessitates a consideration of thickness. A standard method for evaluating the flexibility of a film involves subjecting it to a bending test, wherein the film is affixed to a cylinder with a gradually decreasing radius of curvature until fracture occurs [180]. To quantify this flexibility, Peng et al. [181] introduced the concept of a figure of merit for flexibility (f_{FOM}), which can be elucidated through the yield strain (ε), representing the extent of elastic stretching prior to plastic deformation at a given thickness. The maximum ε, indicative of the degree of elongation on the outer or inner surface can be calculated using the formula $\varepsilon = h/2r$, where *h* denotes the thickness and *r* signifies the minimum bending radius preceding the fracture (Fig. 10a).

When Bi_2Te_3-based films reach a certain level of thinness, they exhibit flexibility. For instance, Fan et al. [114] deposited a 240 nm thick Bi_2Te_3 film through thermal evaporation, resulting in an f_{FOM} of ~2 × 10^{-5}. Shang et al. [107] utilized magnetron sputtering to fabricate a 420 nm-thick Bi_2Te_3 film; however, the f_{FOM} approached only 4 × 10^5 due to its modest thickness and large critical bending radius. Recent advancements include the synthesis of a 30 μm-thick Bi_2Te_3/cellulose fiber film by Jin et al. [111] using magnetron sputtering, and the fabrication of a 40 μm thick Bi_2Te_3/rGO film by Ding et al. [159] employing a printing method. These innovations yielded a further improvement in the f_{FOM} to approximately 1× 10^{-2}. Despite the exhibited flexibility of these Bi_2Te_3-based films, their maximum power output remains severely limited due to the restricted thermal and electronic loading capacity resulting from their small thickness. Therefore, it is imperative to develop thicker Bi_2Te_3-based films while preserving flexibility.

The Bi_2Te_3/CC film demonstrated the highest flexibility among all reported Bi_2Te_3-based composite films (Fig. 10b). Its flexibility surpassed that of Bi_2Te_3 films fabricated via magnetron sputtering [107], thermal evaporation [114], and electrodeposition [120], screen-printed Bi_2Te_3 films [129] and composite films such as Bi_2Te_3/SWCNT [106], Bi_2Te_3/SWCNT [125], Bi_2Te_3/CFF [137], Bi_2Te_3/Graphene [126], Bi_2Te_3/NiFoam [136], Bi_2Te_3/CNF [127] and Bi_2Te_3/rGO films [159], with differences in f_{FOM} ranging from 2 to 3 orders of magnitude. This superiority can be attributed to the outstanding intrinsic flexibility of the CC substrate, which accommodates the bending deformation of Bi_2Te_3 effectively.

4. Optimization mechanisms

Co-optimizing the TE performance and flexibility of Bi_2Te_3-based films is a complex task involving multiple aspects, with the primary aim of enhancing electrical transport properties, reducing the κ, and ensuring excellent flexibility. Enhancing the electrical performance involves adjusting the transport properties, σ, μ, as well as the *S* values for an enhanced *PF*. Below, will explore strategies such as defects control, bridging effect, and energy filtering. For depressing the κ, below, we will explore strategies from aspects of interfacial phonon scattering effect, mixing rule, and independent vibration scattering. For endowing Bi_2Te_3-based films with flexibility, below will detail several key strategies to optimize flexibility and closely related mechanical properties, such as increasing spatial freedom, decreasing slippage barriers, excellent flexibility of guests, knotting effect, and interphase strengthening.

4.1. Enhancing electrical performance

4.1.1. Defects control

Bi_2Te_3-based films inherently possess defects such as heterogeneous atom doping, vacancies, etc. These defects can significantly affect the *n* or μ. Through appropriate fabrication and post-treatment, these defects can be effectively controlled, thereby enhancing the overall electrical performance. Annealing can promote grain growth, thereby reducing grain boundaries and dislocations. Due to the high vapor pressure of Te, Te can easily evaporate during annealing, leading to compositional deviations. Therefore, it is usually carried out in a protective atmosphere, or a Te-rich atmosphere, to suppress the evaporation and oxidation of Te [136,182,183]. This ensures the stoichiometric balance, preventing performance degradation caused by Te deficiency. Additionally, optimizing the annealing temperature and duration is also crucial for reducing defects, as too high annealing temperature or too long duration will lead to excessive Te evaporation.

4.1.2. Bridging effect

The bridging effect plays a crucial role in Bi_2Te_3-based materials by constructing carrier transport channels for optimizing carrier mobility. This mechanism involves introducing high-conducting second-phase materials such as graphene and CNT into the Bi_2Te_3 matrix [126,184]. When these guest phases bridge the Bi_2Te_3-based materials, they create continuous channels or pathways for charge carrier transport [185]. This interconnected network effectively bridges gaps between particles or regions within the composite material, ensuring a more uniform and efficient transport of charge carriers. By establishing these interconnected pathways, the bridging effect minimizes the scattering and trapping of charge carriers at interfaces or defects in the material, leading increased μ (Fig. 10c) [186]. Chen et al. [125] achieved an σ of 244.6 S/cm in the SWCNT/Bi_2Te_3 film, nearly doubling that of pure SWCNT film, due to the bridging effect of CNTs within the Bi_2Te_3 matrix. Shi et al. [136] reported an σ of 1107.8 S/cm in the Bi_2Te_3/NiFoam composite film, attributed to the bridging effect of the nickel framework.

4.1.3. Energy filtering effect

When an energy barrier is established between the guest phases and the Bi_2Te_3 system, it will scatter the low-energy carriers and

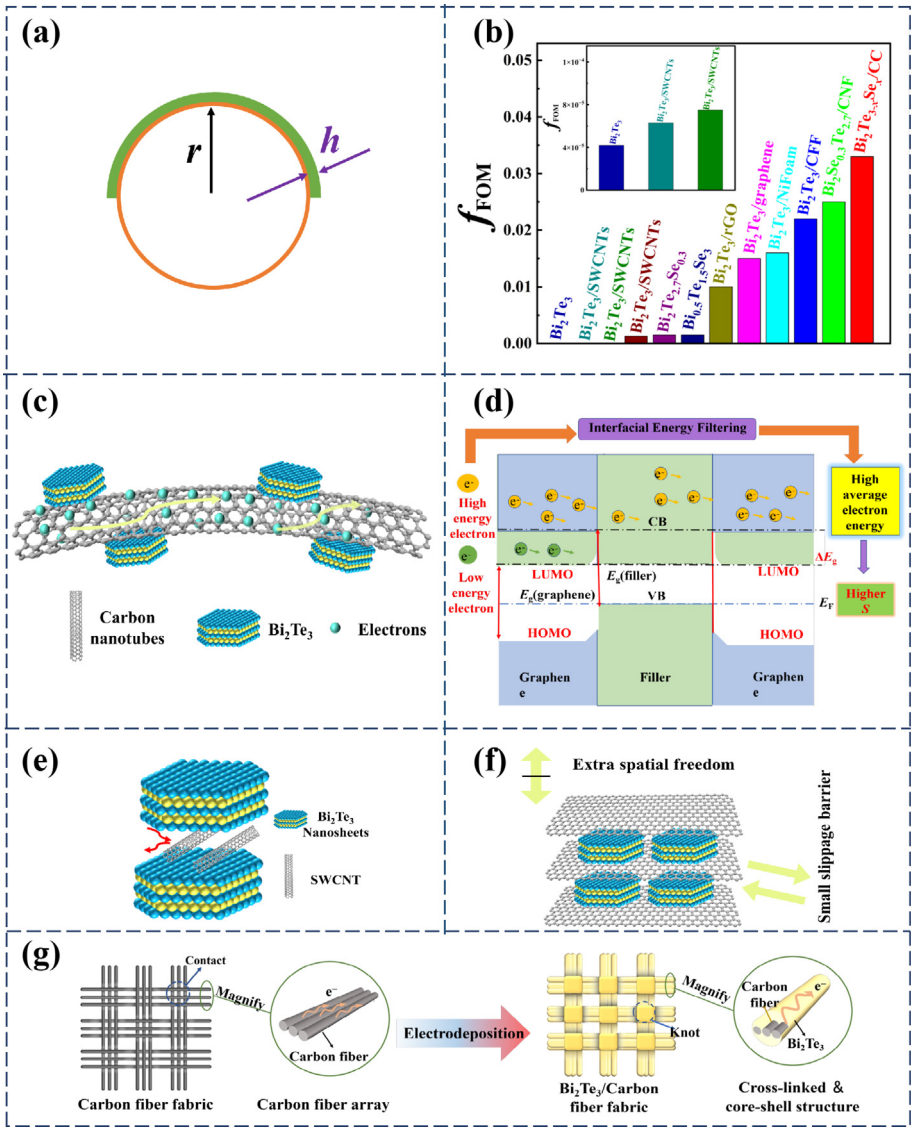

Fig. 10. Flexibility and performance optimization mechanisms of the Bi_2Te_3-based flexible films. (a) Schematic diagram of the definition of f_{FOM}. (b) The reported f_{FOM} values [95,106,125–127,107,136,137,159,176,177]. Schematic diagram of (c) bridging effect, (d) energy filtering effect, (e) interfacial phonon scattering effect, (f) increasing spatial freedom, and decreasing slippage barriers. (g) Knotting effect in cross-linked core-shell structure [137]. Copyright 2022, Elsevier.

impede their transport while letting the high-energy carriers pass through. As the high-energy carriers are the primary contributors for *S*, this selective scattering would thus lead to a remarkably increased *S* [158,187,188]. Mao et al. [126] demonstrated a graphene/Bi_2Te_3 composite film exhibiting significantly enhanced *S*. This improvement is attributed to the establishment of an energy barrier (ΔE_g ~0.2 eV) at the graphene/Bi_2Te_3 interface, resulting from energy transfer between the conduction band (CB) of Bi_2Te_3 and graphene during carrier transport [189]. This energy barrier impedes carriers with energies below ΔE_g while enabling carriers to traverse energies above ΔE_g, as depicted in Fig. 10d [112]. Consequently, there is an elevation in the average energy of the transport carriers, thereby enhancing the *S* [153].

4.2. Depressing thermal conductivity

4.2.1. Interfacial phonon scattering effect

The interfacial phonon scattering effect is a phenomenon where phonons experience scattering at the interfaces between different materials [190]. This effect plays a significant role in determining the κ, particularly at the nanoscale, where interfacial interactions become prominent [191,192]. Bi_2Te_3-based composite materials composed of dissimilar components, such as polymers mixed with inorganic Bi_2Te_3, phonons encounter interfaces between the two phases [193]. These interfaces introduce discontinuities in the crystal lattice, leading to scattering phonons and hindering their propagation. As a result, the overall κ is reduced. The interfacial phonon scattering effect is influenced by factors such as the mismatch in lattice structure, atomic mass, and bonding strength at the interface (Fig. 10e). Well-dispersed Bi_2Te_3-based nanosheets can induce substantial heterointerfaces between Bi_2Te_3-based materials and SWCNTs. Owing to their lattice mismatch, these heterointerfaces effectively scatter phonons during heat transfer, resulting in elevated interfacial thermal resistance [194]. Jin et al. [106] elucidated that within SWCNTs/Bi_2Te_3 hybrids, the discrepancy in phonon spectra at the SWCNTs-Bi_2Te_3 interface can efficiently impede phonon transport across the interface [195,196]. Moreover, the presence of interface roughness and nanoporous structure exacerbates diffusive phonon scattering at the interfaces and boundaries, contributing to a notable reduction in κ_l.

4.2.2. Mixing rule

The mixing rule is a concept used to predict the properties of Bi_2Te_3-based composite materials by considering the properties of their individual components and their relative proportions [197]. It is based on the assumption that the properties of the composite are determined by the properties of its constituents and their arrangement within the material. In the context of κ, the mixing rule can be applied to predict the κ of a Bi_2Te_3-based composite material formed by mixing two or more components [198,199]. In the case of combining organics with Bi_2Te_3-based matrix to form a composite material, the mixing rule can help predict the overall κ based on the thermal conductivities of the organic component (such as PEDOT:PSS) and Bi_2Te_3-based matrix, as well as their volume fractions [200]. The κ of the PEDOT/52 vol% Bi_2Te_3 hybrid film reported by Wang et al. [130] is only ~0.5 W/m/K, which is much lower than that of the Bi_2Te_3 film.

4.2.3. Independent vibration scattering

Independent vibration scattering refers to a phenomenon observed when long-chain organic molecules are bonded to a host layer, such as in the case of $Bi_2Se_3HA_xDMSO_y$ films [201]. These organic molecules exhibit autonomous vibrational motions due to their flexible and extended structure. As phonons, the primary heat carriers in materials, propagate through the host layer, they interact with these vibrating organic chains. This interaction disrupts the coherent movement of phonons, leading to scattering. Because these vibrations occur independently of each other, they create multiple scattering centers throughout the material. As a result, phonon transport is hindered, leading to a significant reduction in κ. In the $Bi_2Se_3HA_xDMSO_y$ material, extended chains of organic molecules are dispersed atop the Bi_2Se_3 layer. These organic moieties introduce phonon scattering, which is attributable to their autonomous vibrational motions. Consequently, this scattering phenomenon leads to a notable reduction in the κ of the $Bi_2Se_3HA_xDMSO_y$ film, declining from the pristine value of 3.37 W/m/K observed for pure Bi_2Se_3 to a diminished level of 1.52 W/m/K.

4.3. Flexibility optimization

4.3.1. Increasing spatial freedom

Incorporating structures that increase spatial freedom within materials is a pivotal strategy for enhancing their flexibility. By creating additional space for deformation, these structures allow materials to bend and flex more readily. The incorporation of a sandwich structure or the inclusion of molecules that expand interlayer spacing introduces additional freedom along the C-axis [126]. The graphene/Bi_2Te_3/graphene sandwich structure, as shown in Fig. 10f, creates additional space for bending deformation [126], allowing the composite to exhibit exceptional flexibility. The incorporation of organic molecules into the vdW gaps between the quintuple layers of Bi_2Se_3 also increased the interlayer spacing within Bi_2Se_3, creating more deformation space, thus significantly improving the flexibility [201].

4.3.2. Decreasing slippage barriers

When a material bends, energy dissipation occurs, and the degree of flexibility is significantly influenced by the interactions at the interface of different layers within the material. Ensuring a small slip barrier at the interface is essential for maintaining excellent flexibility. This is because a low slip barrier facilitates easier sliding motion between adjacent layers, reducing resistance and preventing damage during deformation (Fig. 10f). The graphene/Bi_2Te_3/graphene sandwich structure [126] demonstrated superior flexibility due to the vdW bond between the graphene and Bi_2Te_3 layers. The small sliding barrier at the interface facilitated easy sliding motion between adjacent layers, contributing to the excellent flexibility.

4.3.3. Excellent flexibility of guests

The excellent flexibility of guest phases or templates inherently enhances the flexibility of Bi_2Te_3-based films. For example, combining organics with Bi_2Te_3 systems have been shown to effectively endow the composite films with flexibility [202]. The Bi_2Te_3/CNF films [127] exhibited good flexibility, which was attributed to the flexibility provided by CNF. The $Bi_{0.5}Sb_{1.5}Te_3$-based composite film containing the conductive polymer PEDOT, the strong plasticizer PVA had a tensile strength of 79.3 MPa and a fracture strain of approximately 32.4% [122]. Besides, flexible substrates such as PI or flexible templates could also impart flexibility to Bi_2Te_3-based composites. These substrates/templates provide a supportive yet pliable foundation that accommodates bending and twisting motions.

4.3.4. Knotting effect

The knotting effect refers to the phenomenon where the intertwining of fibers within a Bi_2Te_3-based composite film leads to significant enhancement of its mechanical properties. This effect creates a complex network of physical connections that bolster the strength, toughness, and fatigue resistance. The knotted fibers could create a robust network that can better distribute and absorb stress. This network prevents localized failures, increasing the overall strength. The intricate network formed by knotting could hinder the initiation and propagation of cracks. In the CFF/Bi_2Te_3 composite film with a cross-linked core-shell structure (Fig. 10g) [137], the woven fiber structure of the CFF exemplifies the knotting effect, facilitating stress transfer and increasing the mechanical performance. The tensile strength reached 20.5 MPa, a fourfold increase compared to CFF.

4.3.5. Interphase strengthening

Interphase strengthening involves generating a secondary phase between the original phases to enhance mechanical stability by creating a strong bonding effect at the interfaces. In the Bi_2Te_3/NiFoam composite film [136], an interphase compound, $NiTe_2$, was formed around the nickel skeletons during the annealing process. This interphase $NiTe_2$ acted as a bonding phase between the nickel and Bi_2Te_3 phases. The presence of $NiTe_2$ not only facilitated enhanced carrier transport across the interface but also significantly improved the mechanical stability.

5. Conclusion and outlook

Bi_2Te_3-based materials are widely recognized as the most efficient material for RT TE applications. However, its inherent rigidity has hindered its widespread use in flexible TE conversion systems. Recent research has focused on enhancing the flexibility of Bi_2Te_3-based materials through various methods such as bulk thinning, physical/chemical deposition on flexible substrates, paste casting, and template methods. These efforts have resulted in a notable increase in research publications. This review provides a comprehensive update on synthesis approaches, microstructures, TE performance, flexibility, and the underlying mechanisms. It can be concluded that for enhancing *PF*, one can optimize carrier concentration by defect tuning, design structures to enhance carrier transport by bridging gaps/barriers, or utilize energy-selective interfaces to induce an energy-filtering effect. For suppression of κ, one can utilize interfaces to scatter phonons and incorporate low-κ phases to disrupt phonon propagation, or introduce defects or structures that independently scatter phonons. For flexibility optimization, one can design structures or interfaces that allow for

greater movement or deformation, and reduce constraints that hinder the flexibility, enabling smoother deformation, or incorporating organic components or structures known for their inherent flexibility to enhance the overall flexibility.

Future research directions could include exploring novel deposition/casting techniques, which could open up new avenues for improving flexibility and scalability; further optimizing synthesis/modification methods to enhance flexibility without compromising TE performance; and understanding the underlying mechanisms governing the flexibility-TE performance relationship, which is crucial for the development of high-performance flexible TE materials.

For novel deposition/casting techniques: investigating innovative deposition techniques, such as atomic layer deposition, which could possibly enable the fabrication of flexible Bi_2Te_3 films with precise control over thickness and morphology. Moreover, exploring alternative flexible substrate/template materials beyond traditional ones could offer enhanced mechanical stability and compatibility with diverse application environments.

For synthesis/modification optimization: future research should focus on refining synthesis methods to enhance flexibility while maintaining or even improving their TE performance. This might involve exploring a new second phase, such as novel conductive polymers and additives, refining processing parameters, such as temperature, pressure, and precursor compositions, to tailor the microstructure and mechanical properties for flexibility. Organic interaction is also promising to decouple the adjacent layers of Bi_2Te_3, which may co-enhance the flexibility as well as the TE performance due to various mechanisms.

For an understanding of the flexibility-TE performance relationship: it is essential to delve deeper into the underlying mechanisms governing the relationship between flexibility and TE performance. This could involve comprehensive characterization techniques, including in situ mechanical testing, to elucidate how structural modifications at the nanoscale level impact both the electrical and thermal transport properties of the material under varying degrees of mechanical strain.

Continued research efforts in flexible Bi_2Te_3-based TE systems hold significant promise for practical applications in various fields, including wearable electronics, automotive waste heat recovery, and self-powered sensors. By addressing key challenges related to flexibility, scalability, and performance stability, researchers can accelerate the transition of flexible TE technologies from the laboratory to real-world applications, paving the way for sustainable energy harvesting and thermal management solutions.

CRediT authorship contribution statement

Mengran Chen: Writing – original draft, Investigation. **Zhendong Mao:** Validation, Investigation. **Yuru Ji:** Validation, Investigation. **Peng-an Zong:** Writing – review & editing, Visualization, Supervision, Funding acquisition. **Qihao Zhang:** Writing – review & editing.

Declaration of competing interest

The authors declare that they have no known competing financial interests or personal relationships that could have appeared to influence the work reported in this paper.

Data availability

Data will be made available on request.

Acknowledgments

The authors acknowledge the support from NASF (no. U2230131), the Postgraduate Research & Practice Innovation Program of Jiangsu Province (KYCX23_1396) and the Priority Academic Program Development of Jiangsu Higher Education Institutions (PAPD). Peng-an Zong thanks Dr. Yao Lu from Southern University of Science and Technology for providing the original data (Fig. 3) and also thank Dr. Kafil M. Razeeb from Tyndall National Institute of Ireland for discussion.

References

[1] X.L. Shi, K. Zheng, M. Hong, W.D. Liu, R. Moshwan, Y. Wang, X.L. Qu, Z.G. Chen, J. Zou, Boosting the thermoelectric performance of p-type heavily Cu-doped polycrystalline SnSe via inducing intensive crystal imperfections and defect phonon scattering, Chem. Sci. 9 (37) (2018) 7376–7389, https://doi.org/10.1039/c8sc02397B.

[2] X.L. Shi, K. Zheng, W.D. Liu, Y. Wang, Y.Z. Yang, Z.G. Chen, J. Zou, Realizing high thermoelectric performance in n-type highly distorted Sb-doped SnSe microplates via tuning high electron concentration and inducing intensive crystal defects, Adv. Energy Mater. 8 (21) (2018) 1800775, https://doi.org/10.1002/aenm.201800775.

[3] S.B. Liu, Y. Wen, S.L. Bai, H.N. Shi, Y.X. Qin, B.C. Qin, D.R. Liu, Q. Cao, X. Gao, L.Z. Su, C. Cheng, X. Zhang, L.D. Zhao, Lattice plainification leads to high thermoelectric performance of p-type PbSe crystals, Adv. Mater. (2024) 2401828, https://doi.org/10.1002/adma.202401828.

[4] W.D. Liu, Z.G. Chen, J. Zou, Eco-friendly higher manganese silicide thermoelectric materials: progress and future challenges, Adv. Energy Mater. 8 (9) (2018) 1800056, https://doi.org/10.1002/aenm.201800056.

[5] M.Y. Toriyama, A.N. Carranco, G.J. Snyder, P. Gorai, Material descriptors for thermoelectric performance of narrow-gap semiconductors and semimetals, Mater. Horiz. 10 (10) (2023) 4256–4269, https://doi.org/10.1039/D3MH01013A.

[6] J. Zhou, W. Zhu, Q.Q. Zhang, G.Y. Han, Y.T. Liu, Z.P. Guo, S.M. Guo, Y. Huang, Y. Deng, Enhanced electrical and mechanical properties of Bi_2Te_3-based thermoelectric thick films enabled by a practical dynamic regulation strategy, J. Materiomics 10 (2) (2024) 480–489, https://doi.org/10.1016/j.jmat.2023.07.010.

[7] P.F. Xu, K.P. Jin, Y. Yuan, M. Huang, Z.H. Yan, X. Li, X. Gao, L.W. Fu, B. Xu, High-performance Bi_2Te_3-based thermoelectrics enabled by ≈1 nm metal chalcogenide clusters with size-dependent electron and phonon structures, Adv. Funct. Mater. (2024) 2401240, https://doi.org/10.1002/adfm.202401240.

[8] G. Wu, Q. Zhang, X.J. Tan, Y.T. Fu, Z. Guo, Z.W. Zhang, Q.Q. Sun, Y. Liu, H.L. Shi, J.S. Li, J. Noudem, J.H. Wu, G.Q. Liu, P. Sun, H.Y. Hu, J. Jun, Bi_2Te_3-based thermoelectric modules for efficient and reliable low-grade heat recovery, Adv. Mater. (2024) e2400285, https://doi.org/10.1002/adma.202400285.

[9] Y.Y. Li, X.Y. Qin, D. Li, J. Zhang, C. Li, Y.F. Liu, C.J. Song, H.X. Xin, H.F. Guo, Enhanced thermoelectric performance of $Cu_2Se/Bi_{0.4}Sb_{1.6}Te_3$ nanocomposites at elevated temperatures, Appl. Phys. Lett. 108 (2016) 062104, https://doi.org/10.1063/1.4941757.

[10] F.D. Zhang, L.J. Zhu, M.S. Song, X.F. Cao, X.H. Pang, P.F. Liang, Z.H. Peng, X.L. Chao, Z.P. Yang, D. Wu, Giant deformation induced staggered-layer structure promoting the thermoelectric and mechanical performance in n-type $Bi_2(Te, Se)_3$, small. https://doi.org/10.1002/smll.202401070, 2024.

[11] W.D. Liu, L.C. Yin, L. Li, Q.S. Yang, D.Z. Wang, M. Li, X.L. Shi, Q.F. Liu, Y. Bai, Y. Gentle, L.Z. Wang, Z.G. Chen, Grain boundary re-crystallization and sub-nano regions leading to high plateau figure of merit for Bi_2Te_3 nanoflakes, Energy Environ. Sci. 16 (11) (2023) 5123–5135, https://doi.org/10.1039/d3ee02370B.

[12] W.J. Xie, J. He, H.J. Kang, X.F. Tang, S. Zhu, M. Laver, S.Y. Wang, J.R.D. Copley, C.M. Brown, Q.J. Zhang, T.M. Tritt, Identifying the specific nanostructures responsible for the high thermoelectric performance of $(Bi,Sb)_2Te_3$ nanocomposites, Nano Lett. 10 (9) (2010) 3283–3289, https://doi.org/10.1021/nl100804A.

[13] S.I. Kim, K.H. Lee, H.A. Mun, H.S. Kim, S.W. Hwang, J.W. Roh, D.J. Yang, W.H. Shin, X.S. Li, Y.H. Lee, G.J. Snyder, S.W. Kim, Dense dislocation arrays embedded in grain boundaries for high-performance bulk thermoelectrics, Science 348 (6230) (2015) 109–114, https://doi.org/10.1126/science.aaa4166.

[14] B. Poudel, Q. Hao, Y. Ma, Y.C. Lan, A. Minnich, B. Yu, X.A. Yan, D.Z. Wang, A. Muto, D. Vashaee, X.Y. Chen, J.M. Liu, M.S. Dresselhaus, G. Chen, Z.F. Ren, High-thermoelectric performance of nanostructured bismuth antimony telluride bulk alloys, Science 320 (5876) (2008) 634–638, https://doi.org/10.1126/science.1156446.

[15] Y. Ma, Q. Hao, B. Poudel, Y.C. Lan, Bo Yu, D.Z. Wang, G. Chen, Z.F. Ren, Enhanced thermoelectric figure-of-merit in p-type nanostructured bismuth antimony tellurium alloys made from elemental chunks, Nano Lett. 8 (8) (2008) 2580–2584, https://doi.org/10.1021/nl8009928.

[16] J.H. Li, Q. Tan, J.F. Li, D.W. Liu, F. Li, Z.Y. Li, M.M. Zou, K. Wang, BiSbTe-based nanocomposites with high ZT: the effect of SiC nanodispersion on

thermoelectric properties, Adv. Funct. Mater. 23 (35) (2013) 4317–4323, https://doi.org/10.1002/adfm.201300146.
[17] J.X. Shi, H.L. Chen, S.H. Jia, W.J. Wang, 3D printing fabrication of porous bismuth antimony telluride and study of the thermoelectric properties, J. Manuf. Process. 37 (2019) 370–375, https://doi.org/10.1016/j.jmapro.2018.11.001.
[18] D. Yang, X.L. Shi, L.M. Li, M. Nisar, A. Mansoor, S. Chen, Y. Chen, Y.F. Li, H.L. Ma, G.X. Liang, X.H. Zhang, W.D. Liu, P. Fan, Z.G. Zheng, Z.H. Chen, Flexible power generators by Ag_2Se thin films with record-high thermoelectric performance, Nat. Commun. 15 (1) (2024) 923, https://doi.org/10.1038/s41467-024-45092-7.
[19] Y.X. Zhang, Y. Meng, L.Q. Wang, C.Y. Lan, Q. Quan, W. Wang, Z.X. Lai, W.J. Wang, Y.Z. Li, D. Yin, D.J. Li, P.S. Xie, D. Chen, Z. Yang, S. Yip, Y. Lu, C.Y. Wong, J.C. Ho, Pulse irradiation synthesis of metal chalcogenides on flexible substrates for enhanced photothermoelectric performance, Nat. Commun. 15 (1) (2024) 728, https://doi.org/10.1038/s41467-024-44970-4.
[20] F.K. Guo, Y.X. Sun, H.X. Qin, Y.K. Zhu, Z.H. Ge, Z.H. Liu, W. Cai, J.H. Sui, BiSbTe alloy with high thermoelectric and mechanical performance for power generation, Scripta Mater. 218 (2022) 114801, https://doi.org/10.1016/j.scriptamat.2022.114801.
[21] G.M. Park, S. Lee, J.Y. Kang, S.H. Baek, H. Kim, J.S. Kim, Understanding secondary phase inclusion and composition variations in the microstructure design of n-type Bi_2Te_3 alloys via selective dissolution of KCl, J. Adv. Ceram. 12 (12) (2023) 2360–2370, https://doi.org/10.26599/JAC.2023.9220825.
[22] N.S. Chauhan, S.V. Pyrlin, O.I. Lebedev, L.S.A. Marques, M.M.D. Ramos, T. Maiti, K. Kovnir, B.A. Korgel, Y.V. Kolen'ko, Compositional fluctuations mediated by excess tellurium in bismuth antimony telluride nanocomposites yield high thermoelectric performance, J. Phys. Chem. C 125 (37) (2021) 20184–20194, https://doi.org/10.1021/acs.jpcc.1c05375.
[23] X.M. Hu, Q.S. Xiang, D. Kong, X. Fan, B. Feng, Z. Pan, P.H. Liu, R.S. Li, G.Q. Li, Y.W. Li, The effect of Ni/Sn doping on the thermoelectric properties of BiSbTe polycrystalline bulks, J. Solid State Chem. 277 (2019) 175–181, https://doi.org/10.1016/j.jssc.2019.06.006.
[24] L. Xing, W.J. Cui, X.H. Sang, F.X. Hu, P. Wei, W.T. Zhu, X.L. Nie, Q.J. Zhang, W.Y. Zhao, Enhanced thermoelectric performance and atomic-resolution interfacial structures in BiSbTe thermo-electro-magnetic nanocomposites incorporating magnetocaloric LaFeSi nanoparticles, J. Materiomics 7 (5) (2021) 998–1006, https://doi.org/10.1016/j.jmat.2021.02.013.
[25] D. Zhang, J.D. Lei, W.B. Guan, Z. Ma, C. Wang, L.J. Zhang, Z.X. Cheng, Y.X. Wang, Enhanced thermoelectric performance of BiSbTe alloy: energy filtering effect of nanoprecipitates and the effect of SiC nanoparticles, J. Alloys Compd. 784 (2019) 1276–1283, https://doi.org/10.1016/j.jallcom.2019.01.084.
[26] C. Tan, X.J. Tan, F.F. Shi, Y.O. Yin, G.Q. Liu, C.L. Xiong, H.X. Wang, G.Q. Luo, B. Yu, J.G. Noudem, B. Liang, J. Jiang, Enhanced thermoelectric performance of p-type sintered BiSbTe-based composites with $AgSbTe_2$ addition, Ceram. Int. 47 (2021) 725–731, https://doi.org/10.1016/j.ceramint.2020.08.182.
[27] F.R. Sie, C.S. Hwang, C.H. Kuo, Y.W. Chou, C.H. Yeh, Enhanced thermoelectric properties of p-type BiSbTe/TiO_2Ag alloys, Intermetallics 109 (2019) 30–36, https://doi.org/10.1016/j.intermet.2019.03.001.
[28] P. Sharief, B. Madavali, P. Dharmaiah, J.W. Song, S. Gian, Y. Sohn, J.H. Han, S.H. Song, S.J. Hong, Enhancing the thermoelectric properties of powder metallurgically produced BiSbTe alloy through feasible electroless surface coating method, J. Eur. Ceram. Soc. 42 (2022) 3473–3479, https://doi.org/10.1016/j.jeurceramsoc.2022.02.054.
[29] W.H. Shin, J.W. Roh, B. Ryu, H.J. Chang, H.S. Kim, S. Lee, W.S. Seo, K. Ahn, Enhancing thermoelectric performances of bismuth antimony telluride via synergistic combination of multiscale structuring and band alignment by $FeTe_2$ incorporation, ACS Appl. Mater. Interfaces 10 (2018) 3689–3698, https://doi.org/10.1021/acsami.7b18451.
[30] L.W. Fu, K.H. Lee, S.I. Kim, J.H. Lim, W. Choi, Y.D. Cheng, M.W. Oh, Y.M. Kim, S.W. Kim, Hidden role of intrinsic Sb-rich nano-precipitates for high-performance $Bi_{2-x}Sb_xTe_3$ thermoelectric alloys, Acta Mater. 215 (2021) 117058, https://doi.org/10.1016/j.actamat.2021.117058.
[31] Y.Y. Li, X.C. Wang, G.X. Liu, B.C. Shin, F.K. Shan, High thermoelectric efficiency of p-type BiSbTe-based composites with $CuGaTe_2$ nanoinclusions, Acta Mater. 215 (2021) 117058, https://doi.org/10.1016/j.scriptamat.2019.07.016.
[32] L.W. Fu, K.S. Park, S.I. Kim, B.J. Kim, H.Y. Song, W. Choi, Y.M. Kim, J.Y. Hwang, K.H. Lee, S.W. Kim, High-performance bismuth antimony telluride thermoelectric membrane on curved and flexible supports, ACS Energy Lett. 6 (2021) 2378–2385, https://doi.org/10.1021/acsenergylett.1c00801.
[33] H.X. Qin, W.B. Qu, Y. Zhang, Y.S. Zhang, Z.H. Liu, Q. Zhang, H.J. Wu, W. Cai, J.H. Sui, Nanotwins strengthening high thermoelectric performance bismuth antimony telluride alloys, Adv. Sci. 9 (14) (2022) 2200432, https://doi.org/10.1002/advs.202200432.
[34] P. Dharmaiah, D.H. Kim, J.G. Kwon, Y. Lee, S. Geum, G.R. Lee, M. Kang, S.J. Hong, Optimization of mixed grain size structure for enhancement of thermoelectric figure of merit in p-type BiSbTe-based alloys, J. Mater. Sci. 57 (38) (2022) 18131–18141, https://doi.org/10.1007/s10853-022-07532-x.
[35] J.Y. Lim, S. Cho, H. Kim, Y. Seo, Optimum thermoelectric performance of bismuth–antimony–telluride alloy/PEDOT:PSS nanocomposites prepared by an innovative redox process, ACS Appl. Energy Mater. 2 (11) (2019) 8219–8228, https://doi.org/10.1021/acsaem.9b01702.
[36] P. Zhao, F.R. Yu, B.H. Wang, H.D. Zhao, C. Chen, D. Wang, P. Ying, Y.J. Wu, P.H. Li, B. Zhang, B. Liu, Z.S. Zhao, W.T. Hu, D.L. Yu, J. He, Z. Liu, B. Xu, Y.J. Tian, Porous bismuth antimony telluride alloys with excellent thermoelectric and mechanical properties, J. Mater. Chem. A 9 (8) (2021) 4990–4999, https://doi.org/10.1039/d0ta09795k.
[37] Z.C. Wei, C.Y. Wang, J.Y. Zhang, J. Yang, Z.L. Li, Q.D. Zhang, P.F. Luo, W.Q. Zhang, E.K. Liu, J. Luo, Precise regulation of carrier concentration in thermoelectric BiSbTe alloys via magnetic doping, ACS Appl. Mater. Interfaces 12 (2020) 20653–20663, https://doi.org/10.1021/acsami.0c02408.
[38] G.S. Yang, L.N. Sang, F.F. Yun, D.R.G. Mitchell, G. Casillas, N. Ye, K. See, J. Pei, X.G. Wang, J.F. Li, G.J. Snyder, X. Wang, Significant enhancement of thermoelectric figure of merit in BiSbTe-based composites by incorporating carbon microfiber, Adv. Funct. Mater. 31 (15) (2021) 2008851, https://doi.org/10.1002/adfm.202008851.
[39] C.H. Lee, P. Dharmaiah, D.H. Kim, D.K. Yoon, T.H. Kim, S.H. Song, S.J. Hong, Synergistic optimization of the thermoelectric and mechanical properties of large-size homogeneous $Bi_{0.5}Sb_{1.5}Te_3$ bulk samples via carrier engineering for efficient energy harvesting, ACS Appl. Mater. Interfaces 14 (8) (2022) 10394–10406, https://doi.org/10.1021/acsami.1c23736.
[40] M. Bumrungpon, K. Hirota, K. Takagi, K. Hanasaku, T. Hirai, I. Morioka, R. Yasufuku, M. Kitamura, K. Hasezaki, Synthesis and thermoelectric properties of bismuth antimony telluride thermoelectric materials fabricated at various ballmilling speeds with yttria-stabilized zirconia ceramic vessel and balls, Ceram. Int. 46 (9) (2020) 13869–13876, https://doi.org/10.1016/j.ceramint.2020.02.180.
[41] H.L. Zhuang, J. Pei, B.W. Cai, J.F. Dong, H.H. Hu, F.H. Sun, Y. Pan, G.J. Snyder, J.F. Li, Thermoelectric performance enhancement in BiSbTe alloy by microstructure modulation via cyclic spark plasma sintering with liquid phase, Adv. Funct. Mater. 31 (2021) 2009681, https://doi.org/10.1002/adfm.202009681.
[42] D.Y. Bao, Q. Sun, L.S. Huang, J. Chen, J. Tang, D.L. Zhou, M. Hong, L. Yang, Z.G. Chen, Thermoelectric performance of p-type $(Bi,Sb)_2Te_3$ incorporating amorphous Sb_2S_3 nanospheres, Chem. Eng. J. 430 (1) (2022) 132738, https://doi.org/10.1016/j.cej.2021.132738.
[43] F. Wu, W. Wang, Thermoelectric properties of n-type $Bi_2Se_{0.3}Te_{2.7}$-based alloys with nanoflowers morphology, Appl. Phys. A 128 (8) (2022) 675, https://doi.org/10.1007/s00339-022-05838-w.
[44] U.G. Hwang, K. Kim, W. Kim, W.H. Shin, W.S. Seo, Y.S. Lim, Thermoelectric transport properties of interface-controlled p-type bismuth antimony telluride composites by reduced graphene oxide, Electron. Mater. Lett. 15 (5) (2019) 605–612, https://doi.org/10.1007/s13391-019-00118-x.
[45] G.S. Yang, R.M. Niu, L.N. Sang, X.Z. Liao, D.R.G. Mitchell, N. Ye, J. Pei, J.F. Li, X.L. Wang, Ultra-high thermoelectric performance in bulk BiSbTe/amorphous boron composites with nano-defect architectures, Adv. Energy Mater. 10 (41) (2020) 2000757, https://doi.org/10.1002/aenm.202000757.
[46] B. Madavali, D.W. Shin, S.H. Song, D.S. Kim, J.K. Lee, S.J. Hong, Preparation and thermoelectric performance of nano rare-earth oxides dispersed p-type BiSbTe alloys by mechanical milling and spark plasma sintering, Mater. Chem. Phys. 253 (2020) 123378, https://doi.org/10.1016/j.matchemphys.2020.123378.
[47] B. Madavali, P. Sharief, K.T. Park, G. Song, S.Y. Back, J.S. Rhyee, S.J. Hong, Development of high-performance thermoelectric materials by microstructure control of p-type BiSbTe based alloys fabricated by water atomization, Materials 14 (17) (2021) 4870, https://doi.org/10.3390/ma14174870.
[48] A. Nozariasbmarz, D. Vashaee, Effect of microwave processing and glass inclusions on thermoelectric properties of p-type bismuth antimony telluride alloys for wearable applications, Energies 13 (17) (2020) 4524, https://doi.org/10.3390/en13174524.
[49] C.H. Zhang, X.J. Geng, B. Chen, J.Q. Li, A. Meledin, L.P. Hu, F.S. Liu, J.G. Shi, J. Mayer, M. Wuttig, O. Cojocaru-Miredin, Y. Yu, Boron-mediated grain boundary engineering enables simultaneous improvement of thermoelectric and mechanical properties in n-type Bi_2Te_3, Small 17 (2021) 2104067, https://doi.org/10.1002/smll.202104067.
[50] C. Kim, D.H. Lopez, Energy filtering and phonon scattering effects in Bi_2Te_3-PEDOT:PSS composite resulting in enhanced n-type thermoelectric performance, Appl. Phys. Lett. 120 (6) (2022) 063903, https://doi.org/10.1063/5.0076952.
[51] M.K. Han, J. Hwang, S.J. Kim, Improved thermoelectric properties of n-type Bi_2Te_3 alloy deriving from two-phased heterostructure by the reduction of CuI with Sn, J. Mater. Sci. Mater. Electron. 30 (2019) 1282–1291, https://doi.org/10.1007/s10854-018-0396-z.
[52] B. Chen, J.Q. Li, M.N. Wu, L.P. Hu, F.S. Liu, W.Q. Ao, Y. Li, H.P. Xie, C.H. Zhang, Simultaneous enhancement of the thermoelectric and mechanical performance in one-step sintered n-type Bi_2Te_3-based alloys via a facile MgB_2 doping strategy, ACS Appl. Mater. Interfaces 11 (2019) 45746–45754, https://doi.org/10.1021/acsami.9b16781.
[53] L.Y. Lou, J. Yang, Y.K. Zhu, H. Liang, Y.X. Zhang, J. Feng, J. He, Z.H. Ge, L.D. Zhao, Tunable electrical conductivity and simultaneously enhanced thermoelectric and mechanical properties in n-type Bi_2Te_3, Adv. Sci. 9 (27) (2022) 2203250, https://doi.org/10.1002/advs.202203250.
[54] C.L. Xiong, F.F. Shi, H.X. Wang, J.F. Cai, S.M. Zhao, X.J. Tan, H.Y. Hu, G.Q. Liu, J.G. Noudem, J. Jiang, Achieving high thermoelectric performance of n-type $Bi_2Te_{2.79}Se_{0.21}$ sintered materials by hot-stacked deformation, ACS Appl. Mater. Interfaces 13 (13) (2021) 15429–15436, https://doi.org/10.1021/acsami.1c02417.
[55] B. Jabar, X. Qin, A. Mansoor, H. Ming, L. Huang, M.H. Danish, J. Zhang, D. Li, C. Zhu, H. Xin, C. Song, Enhanced power factor and thermoelectric

performance for n-type $Bi_2Te_{2.7}Se_{0.3}$ based composites incorporated with 3D topological insulator nanoinclusions, Nano Energy. 80 (2021) 105512, https://doi.org/10.1016/j.nanoen.2020.105512.
[56] B. Jabar, X.Y. Qin, A. Mansoor, H.W. Ming, L.L. Huang, J. Zhang, M.H. Danish, D. Li, C. Zhu, J.H. Zhang, H.X. Xin, C.J. Song, Enhanced thermoelectric performance of n-type $Sn_xBi_2Te_{2.7}Se_{0.3}$ based composites embedded with in-situ formed SnBi and Te nanoinclusions, Compos. B Eng. 197 (2020) 108151, https://doi.org/10.1016/j.compositesb.2020.108151.
[57] X. Chen, F.G. Cai, R. Dong, X.B. Lei, R.Q. Sui, L.X. Qiu, Z.L. Zeng, W. Sun, H. Zheng, Q.Y. Zhang, Enhanced thermoelectric properties of n-type $Bi_2Te_{2.7}Se_{0.3}$ for power generation, J. Mater. Sci. Mater. Electron. 31 (2020) 4924–4930, https://doi.org/10.1007/s10854-020-03057-8.
[58] Q. Zhang, Y.J. Lin, N. Lin, Y. Yu, F. Liu, C.G. Fu, B.H. Ge, O. Cojocaru-Miredin, T.J. Zhu, X.B. Zhao, Enhancing the room temperature thermoelectric performance of n-type Bismuth-telluride-based polycrystalline materials by low-angle grain boundaries, Mater. Today Phys. 22 (2022) 100573, https://doi.org/10.1016/j.mtphys.2021.100573.
[59] T. Chen, H.W. Ming, X.Y. Qin, C. Zhu, Y. Chen, L. Ai, D. Li, Y.S. Zhang, H. Xin, J. Zhang, Enhancing the thermoelectric performance of n-type $Bi_2Te_{2.7}Se_{0.3}$ through the incorporation of Ag_9AlSe_6 inclusions, Inorg. Chem. Front. 9 (2022) 5386–5393, https://doi.org/10.1039/D2QI01232D.
[60] Y.H. Wu, Y. Yu, Q. Zhang, T.J. Zhu, R.S. Zhai, X.B. Zhao, Liquid-phase hot deformation to enhance thermoelectric performance of n-type bismuth-telluride-based solid solutions, Adv. Sci. 6 (21) (2019) 1901702, https://doi.org/10.1002/advs.201901702.
[61] S.J. Jung, B.H. Lee, S.O. Won, S.K. Kim, H.H. Park, J.S. Kim, S.H. Baek, Mapping thermoelectric properties of polycrystalline n-type $Bi_2Te_{3-x}Se_x$ alloys by composition and doping level, J. Alloys Compd. 844 (2020) 155828, https://doi.org/10.1016/j.jallcom.2020.155828.
[62] Y.K. Zhu, Y.X. Sun, J.B. Zhu, K. Song, Z. Liu, M.C. Liu, M. Guo, X.Y. Dong, F.K. Guo, X.J. Tan, B. Yu, W. Cai, J. Jiang, J.H. Sui, Mediating point defects endows n-type Bi_2Te_3 with high thermoelectric performance and superior mechanical robustness for power generation application, Small 18 (23) (2022) 2201352, https://doi.org/10.1002/smll.202201352.
[63] C.L. Chen, T.H. Wang, Z.G. Yu, Y. Hutabalian, R.K. Vankayala, C.C. Chen, W.P. Hsieh, H.T. Jeng, D.H. Wei, Y.Y. Chen, Modulation doping enables ultrahigh power factor and thermoelectric zT in n-type $Bi_2Te_{2.7}Se_{0.3}$, Adv. Sci. 9 (20) (2022) 2201353, https://doi.org/10.1002/advs.202201353.
[64] J.H. Son, M.W. Oh, B.S. Kim, S.D. Park, Optimization of thermoelectric properties of n-type $Bi_2(Te,Se)_2$ with optimizing ball milling time, Rare Met. 37 (4) (2018) 351–359, https://doi.org/10.1007/s12598-018-1028-8.
[65] B. Zhu, W. Wang, J. Cui, J.Q. He, Point defect engineering: co-doping synergy realizing superior performance in n-type Bi_2Te_3 thermoelectric materials, Small 17 (29) (2021) 2101328, https://doi.org/10.1002/smll.202101328.
[66] Q.R. Tao, H.J. Wu, W.F. Pan, Z.Z. Zhang, Y.F. Tang, Y.T. Wu, R.J. Fan, Z.Q. Chen, J.S. Wu, X.L. Su, X.F. Tang, Removing the oxygen-induced donor-like effect for high thermoelectric performance in n-type Bi_2Te_3-based compounds, ACS Appl. Mater. Interfaces 13 (50) (2021) 60216–60226, https://doi.org/10.1021/acsami.1c19357.
[67] Y.K. Zhu, J. Guo, L. Chen, S.W. Gu, Y.X. Zhang, Q. Shan, J. Feng, Z.H. Ge, Simultaneous enhancement of thermoelectric performance and mechanical properties in Bi_2Te_3 via Ru compositing, Chem. Eng. J. 407 (2021) 126407, https://doi.org/10.1016/j.cej.2020.126407.
[68] Y.X. Sun, H.X. Qin, W. Wang, F.K. Guo, W.H. Cai, J.H. Sui, Simultaneous regulation of electrical and thermal transport properties of n-type Bi_2Te_3 via adding excessive te followed by Se doping, ACS Appl. Energy Mater. 4 (5) (2021) 4986–4992, https://doi.org/10.1021/acsaem.1c00546.
[69] C.H. Zhang, C.X. Zhang, H. Ng, Q.H. Xiong, Solution-processed n-type $Bi_2Te_{3-x}Se_x$ nanocomposites with enhanced thermoelectric performance via liquid-phase sintering, Sci. China Mater. 62 (3) (2019) 389–398, https://doi.org/10.1007/s40843-018-9312-5.
[70] Y.S. Wudil, M.A. Gondal, S.G. Rao, S. Kunwar, A.Q. Alsayoud, Substrate temperature-dependent thermoelectric figure of merit of nanocrystalline Bi_2Te_3 and $Bi_2Te_{2.7}Se_{0.3}$ prepared using pulsed laser deposition supported by DFT study, Ceram. Int. 46 (15) (2020) 24162–24172, https://doi.org/10.1016/j.ceramint.2020.06.196.
[71] J.H. Zhang, H.W. Ming, D. Li, X.Y. Qin, J. Zhang, L.L. Huang, C.J. Song, L. Wang, Ultralow thermal conductivity and high thermoelectric performance of n-type $Bi_2Te_{2.7}Se_{0.3}$-based composites incorporated with GaAs nanoinclusions, ACS Appl. Mater. Interfaces 12 (33) (2020) 37155–37163, https://doi.org/10.1021/acsami.0c09338.
[72] I. Malik, T. Srivastava, K.K. Surthi, C. Gayner, K.K. Kar, Enhanced thermoelectric performance of n-type Bi_2Te_3 alloyed with low cost and highly abundant sulfur, Mater. Chem. Phys. 255 (2020) 123598, https://doi.org/10.1016/j.matchemphys.2020.123598.
[73] X.L. Hu, X.A. Fan, B. Feng, D. Kong, P.H. Liu, R.S. Li, Y.L. Zhang, G.Q. Li, Y.W. Li, Equal channel angular extrusion: an effective method to refine the microstructure of cast n-type Bi_2Te_3 based ingot to co-optimize thermoelectric and mechanical properties, Solid State Sci. 103 (2020) 106191, https://doi.org/10.1016/j.solidstatesciences.2020.106191.
[74] X.H. Xiong, L. Zhu, G.X. Wang, D.H. Liu, Q.X. Zhang, W. Feng, Microstructure and properties of n-type Bi_2Te_3 based thermoelectric material fabricated by selective laser sintering, Mater. Res. Express 7 (6) (2020) 066504, https://doi.org/10.1088/2053-1591/ab81be.
[75] O. Meroz, N. Elkabets, Y. Gelbstein, Enhanced thermoelectric properties of n-type $Bi_2Te_{3-x}Se_x$ alloys following melt-spinning, ACS Appl. Energy Mater. 3 (3) (2020) 2090–2095, https://doi.org/10.1021/acsaem.9b02133.
[76] M. Sun, P.Y. Zhang, G.W. Tang, D.D. Chen, Q. Qian, Z.M. Yang, High-performance n-type Bi_2Te_3 thermoelectric fibers with oriented crystal nanosheets, Nanomaterials 13 (2) (2023) 326, https://doi.org/10.3390/nano13020326.
[77] Y.C. Li, S.L. Bi, Y. Wen, Z. Zhao, Zhe, L. Wang, S.B. Liu, J.Q. Zheng, S.Q. Wang, S. Liu, D.Z. Gao, D.R. Liu, Y.C. Zhu, Q. Cao, Qian, X. Gao, Xiang, H.Y. Xie, L.D. Zhao, Realizing high-efficiency thermoelectric module by suppressing donor-like effect and improving preferred orientation in n-type $Bi_2(Te, Se)_3$, Sci. Bull. (2024) 34, https://doi.org/10.1016/j.scib.2024.04.034.
[78] L. Hao, J.H. Feng, L.H. Zhao, E. Min, H.C. Zhang, A. Li, J. Li, R.H. Liu, Hierarchical low-temperature n-type Bi_2Te_3 with high thermoelectric performances, ACS Appl. Mater. Interfaces 16 (17) (2024) 22147–22154, https://doi.org/10.1021/acsami.4c02141.
[79] G. Wu, Q. Zhang, X.J. Tan, Y.T. Fu, Z. Guo, Z.W. Zhang, Q.Q. Sun, Y. Liu, H.L. Shi, J.S. Li, J.G. Noudem, Wu, J.H. Wu, G.Q. Liu, P. Sun, H.Y. Hu, J. Jiang, Bi_2Te_3-Based thermoelectric modules for efficient and reliable low-grade heat recovery, Adv. Mater. (2024) 00285, https://doi.org/10.1002/adma.202400285.
[80] S.B. Liu, Y. Wen, S.L. Bai, H.A. Shi, Y.X. Qin, B.C. Qin, D.R. Liu, Q. Cao, X. Gao, L.Z. Su, C. Chang, X. Zhang, L.D. Zhao, Lattice plainification leads to high thermoelectric performance of P-type PbSe crystals, Adv. Mater. (2024) 01828, https://doi.org/10.1002/adma.202401828.
[81] J.Y. Huang, R.B. Ambade, J. Lombardo, B. Brooks, A. Poosapati, P. Banerjee, M. Saeidi-Javash, Y.L. Zhang, D. Madan, Energy density enhancement of scalable thermoelectric devices using a low thermal budget method with film thickness variation, Appl. Mater. Today 37 (2024) 102116, https://doi.org/10.1016/j.apmt.2024.102116.
[82] M. Hong, Y. Wang, W.D. Liu, S. Matsumura, H. Wang, J. Zou, Z.G. Chen, Arrays of planar vacancies in superior thermoelectric $Ge_{1-x-y}Cd_xBi_yTe$ with band convergence, Adv. Energy Mater. 8 (30) (2018) 1801837, https://doi.org/10.1002/aenm.201801837.
[83] M. Hong, Y. Wang, T.L. Feng, Q. Sun, S.D. Xu, S. Matsumura, S.T. Pantelides, J. Zou, Z.G. Chen, Strong phonon–phonon interactions securing extraordinary thermoelectric $Ge_{1-x}Sb_xTe$ with Zn-alloying-induced band alignment, J. Am. Chem. Soc. 141 (41) (2019) 1742–1748, https://doi.org/10.1021/jacs.8b12624.
[84] Y. Bai, H. Yu, Z. Li, R. Amal, G.Q. Lu, L.Z. Wang, In situ growth of a ZnO nanowire network within a TiO_2 nanoparticle film for enhanced dye-sensitized solar cell performance, Adv. Mater. 24 (43) (2012) 5850–5856, https://doi.org/10.1002/adma.201201992.
[85] D. Yang, X.L. Shi, L.M. Li, M. Nisar, A. Mansoor, S. Chen, Y. Chen, Y.F. Li, H.L. Ma, G.X. Liang, X.H. Zhang, W.D. Liu, P. Fan, Z.G. Zheng, Z.H. Chen, Flexible power generators by Ag_2Se thin films with record-high thermoelectric performance, Nat. Commun. 15 (1) (2024) 923, https://doi.org/10.1038/s41467-024-45092-7.
[86] Y.X. Zhang, Y. Meng, L.Q. Wang, C.Y. Lan, Q. Quan, W. Wang, Z.X. Lai, W.J. Wang, Y.Z. Li, D. Yin, D.J. Li, P.S. Xie, D. Chen, Z. Yang, S. Yip, Y. Lu, C.Y. Wong, J.C. Ho, Pulse irradiation synthesis of metal chalcogenides on flexible substrates for enhanced photothermoelectric performance, Nat. Commun. 15 (1) (2024) 728, https://doi.org/10.1038/s41467-024-44970-4.
[87] B.H. Le, S.R. Zhao, X.H. Liu, S.Y. Woo, G.A. Botton, Z.T. Mi, Controlled coalescence of AlGaN nanowire arrays: an architecture for nearly dislocation-free planar ultraviolet photonic device applications, Adv. Mater. 28 (28) (2016) 8446–8454, https://doi.org/10.1002/adma.201602645.
[88] X.F. Tang, Z.W. Li, W. Liu, Q.J. Zhang, C. Uher, A comprehensive review on Bi_2Te_3-based thin films: thermoelectrics and beyond, Interdisciplinary Materials. 1 (1) (2022) 88–115, https://doi.org/10.1002/idm2.12009.
[89] Y. Saberi, S.A. Sajjadi, A comprehensive review on the effects of doping process on the thermoelectric properties of Bi_2Te_3 based alloys, J. Alloys Compd. 904 (2022) 163918, https://doi.org/10.1016/j.jallcom.2022.163918.
[90] C.S. Kim, G.S. Lee, H. Choi, Y.J. Kim, H.M. Yang, S.H. Lim, S.G. Lee, B.J. Cho, Structural design of a flexible thermoelectric power generator for wearable applications, Appl. Energy 214 (2018) 131–138, https://doi.org/10.1016/j.apenergy.2018.01.074.
[91] D. Madan, Z.Q. Wang, A. Chen, R.C. Juang, J. Keist, P.K. Wright, J.W. Evans, Enhanced performance of dispenser printed MA n-type Bi_2Te_3 composite thermoelectric generators, ACS Appl. Mater. Interfaces 4 (11) (2012) 6117–6124, https://doi.org/10.1021/am301759a.
[92] D. Madan, Z.Q. Wang, A. Chen, P.K. Wright, J.W. Evans, High-performance dispenser printed MA p-type $Bi_{0.5}Sb_{1.5}Te_3$ flexible thermoelectric generators for powering wireless sensor networks, ACS Appl. Mater. Interfaces 5 (22) (2013) 11872–11876, https://doi.org/10.1021/am403568t.
[93] L.L. Zhang, G. Wang, Y.B. Zhang, Z.P. Cao, Y. Wang, T.J. Cao, C. Wang, B. Cheng, W.Q. Zhang, X.G. Wan, J.H. Lin, S.J. Liang, F. Miao, Tuning electrical conductance in bilayer MoS_2 through defect-mediated interlayer chemical bonding, ACS Nano. 14 (8) (2020) 10265–10275, https://doi.org/10.1021/acsnano.0c03665.
[94] K.R. Paton, E. Varrla, C. Backes, R.J. Smith, U. Khan, A. O'Neill, C. Boland, M. Lotya, O.M. Istrate, P. King, T. Higgins, S. Barwich, P. May, P. Puczkarski, I. Ahmed, M. Moebius, H. Pettersson, E. Long, J. Coelho, S.E. O'Brien, E.K. McGuire, B.M. Sanchez, G.S. Duesberg, N. McEvoy, T.J. Pennycook, C. Downing, A. Crossley, V. Nicolosi, J.N. Coleman, Scalable production of large quantities of defect-free few-layer graphene by shear exfoliation in

liquids, Nat. Mater. 13 (6) (2014) 624–630, https://doi.org/10.1038/NMAT3944.
[95] Y. Lu, Y. Zhou, W. Wang, M.Y. Hu, X.G. Huang, D.S. Mao, S. Huang, L. Xie, P.J. Lin, B.B. Jiang, B. Zhu, J.H. Feng, J.X. Shi, Q. Lou, Y. Huang, J.M. Yang, J.H. Li, G.D. Li, J.Q. He, Staggered-layer-boosted flexible Bi_2Te_3 films with high thermoelectric performance, Nat. Nanotechnol. 18 (11) (2023) 1281, https://doi.org/10.1038/s41565-023-01457-5.
[96] P. Nuthongkum, A. Sakulkalavek, R. Sakdanuphab, RSM base study of the effect of argon gas flow rate and annealing temperature on the [Bi]:[Te] ratio and thermoelectric properties of flexible Bi-Te thin film, J. Electron. Mater. 46 (5) (2017) 2900–2907, https://doi.org/10.1007/s11664-016-5024-1.
[97] P. Fan, W.F. Fan, Z.H. Zheng, Y. Zhang, J.H. Luo, G.X. Liang, D.P. Zhang, Thermoelectric properties of zinc antimonide thin film deposited on flexible polyimide substrate by RF magnetron sputtering, J. Mater. Sci. 25 (11) (2014) 5060–5065, https://doi.org/10.1007/s10854-014-2271-x.
[98] R. Feng, F. Tang, N. Zhang, X.H. Wang, Flexible, high-power density, wearable thermoelectric nanogenerator and self-powered temperature sensor, ACS Appl. Mater. Interfaces 11 (42) (2019) 38616–38624, https://doi.org/10.1021/acsami.9b11435.
[99] Z.H. Dong, Q.P. He, D.W. Shen, Z. Gong, D.Y. Zhang, W.Q. Zhang, T. Ono, Y.G. Jiang, Microfabrication of functional polyimide films and microstructures for flexible MEMS applications, Microsyst. Nanoeng. 9 (1) (2023) 31, https://doi.org/10.1038/s41378-023-00503-5.
[100] Y.N. Fang, J.G.D. Hester, B. deGlee, C.C. Tuan, P.D. Brooke, T.R. Le, C. Wong, M.M. Tentzeris, K.H. Sandhage, A novel, facile, layer-by-layer substrate surface modification for the fabrication of all-inkjet-printed flexible electronic devices on Kapton, J. Mater. Chem. C 4 (29) (2016) 7052–7060, https://doi.org/10.1039/C6TC01066K.
[101] Y.N. Fang, J.G.D. Hester, W.J. Su, J.H. Chow, S.K. Sitaraman, M.M. Tentzeris, A bio-enabled maximally mild layer-by-layer Kapton surface modification approach for the fabrication of all-inkjet-printed flexible electronic devices, Sci. Rep. 6 (2016) 39909, https://doi.org/10.1038/srep39909.
[102] I. Gouzman, O. Girshevitz, E. Grossman, N. Eliaz, C.N. Sukenik, Thin film oxide barrier layers: protection of kapton from space environment by liquid phase deposition of titanium oxide, ACS Appl. Mater. Interfaces 2 (7) (2012) 1853, https://doi.org/10.1021/am100113t, 1843.
[103] M. Akram, K.M.B. Jansen, L.J. Ernst, S. Bhowmik, G. Ajeesh, S. Ahmed, D. Chakraborty, Effect of atmospheric pressure plasma modification on polyimide and adhesive joining with titanium, Metall. Mater. Trans. A 46A (10) (2015) 4680–4687, https://doi.org/10.1007/s11661-015-3067-1.
[104] P. Nuthongkum, R. Sakdanuphab, M. Horprathum, A. Sakulkalavek, [Bi]:[Te] Control, Structural and thermoelectric properties of flexible Bi_xTe_y thin films prepared by RF magnetron sputtering at different sputtering pressures, J. Electron. Mater. 46 (2017) 6444–6450, https://doi.org/10.1007/s11664-017-5671-x.
[105] A.N. Pargellis, Evaporating and sputtering: substrate heating dependence on deposition rate, J. Vac. Sci. Technol. A 7 (1) (1989) 27–30, https://doi.org/10.1116/1.575762.
[106] Q. Jin, S. Jiang, Y. Zhao, D. Wang, J.H. Qiu, D.M. Tang, J. Tan, D.M. Sun, P.X. Hou, X.Q. Chen, K.P. Tai, N. Gao, C. Liu, H.M. Cheng, X. Jiang, Flexible layer-structured Bi_2Te_3 thermoelectric on a carbon nanotube scaffold, Nat. Mater. 18 (1) (2019) 62, https://doi.org/10.1038/s41563-018-0217-z.
[107] H.J. Shang, C.C. Dun, Y. Deng, T.G. Li, Z.S. Gao, L.Y. Xiao, H.W. Gu, D.J. Singh, Z.F. Ren, F.Z. Ding, $Bi_{0.5}Sb_{1.5}Te_3$-based films for flexible thermoelectric devices, J. Mater. Chem. A 8 (8) (2020) 4552–4561, https://doi.org/10.1039/c9ta13152c.
[108] Y. Sun, E. Zhang, S. Johnsen, M. Sillassen, P. Sun, F. Steglich, J. Bøttiger, B.B. Iversen, Growth of $FeSb_2$ thin films by magnetron sputtering, Thin Solid Films. 519 (16) (2011) 5397–5402, https://doi.org/10.1016/j.tsf.2011.02.053.
[109] F.H. Hsu, N.F. Wang, Y.Z. Tsai, M.C. Chuang, Y.S. Cheng, M.P. Houng, Study of working pressure on the optoelectrical properties of Al-Y codoped ZnO thin-film deposited using DC magnetron sputtering for solar cell applications, Appl. Surf. Sci. 280 (2013) 104–108, https://doi.org/10.1016/j.apsusc.2013.04.103.
[110] D.Y. Kong, W. Zhu, Z.P. Guo, Y. Deng, High-performance flexible Bi_2Te_3 films based wearable thermoelectric generator for energy harvesting, Inside Energy. 175 (2019) 292–299, https://doi.org/10.1016/j.energy.2019.03.060.
[111] Q. Jin, W.B. Shi, Y. Zhao, J.X. Qiao, J.H. Qiu, C. Sun, H. Lei, K.P. Tai, X. Jiang, Cellulose fiber-based hierarchical porous bismuth telluride for high-performance flexible and tailorable thermoelectrics, ACS Appl. Mater. Interfaces 10 (2) (2018) 1743–1751, https://doi.org/10.1021/acsami.7b16356.
[112] Y. Wang, L. Yang, X.L. Shi, X. Shi, L.D. Chen, M.S. Dargusch, J. Zou, Z.G. Chen, Flexible thermoelectric materials and generators: challenges and innovations, Adv. Mater. 31 (29) (2019) 1807916, https://doi.org/10.1002/adma.201807916.
[113] L.M. Goncalves, C. Couto, P. Alpuim, A.G. Rolo, F. Volklein, J.H. Correia, Optimization of thermoelectric properties on Bi_2Te_3 thin films deposited by thermal co-evaporation, Thin Solid Films. 518 (10) (2010) 2816–2821, https://doi.org/10.1016/j.tsf.2009.08.038.
[114] P. Fan, P.C. Zhang, G.X. Liang, F. Li, Y.X. Chen, J.T. Luo, X.H. Zhang, S. Chen, Z.H. Zheng, High-performance bismuth telluride thermoelectric thin films fabricated by using the two-step single-source thermal evaporation, J. Alloys Compd. 819 (2020) 153027, https://doi.org/10.1016/j.jallcom.2019.153027.
[115] Z.H. Zheng, Y.M. Zhong, Y.L. Li, M. Nisar, A. Mansoor, F. Li, S. Chen, G.X. Liang, P. Fan, D.Y. Xu, M. Wei, Y.X. Chen, Ultrahigh thermoelectric properties of p-type $Bi_xSb_{2-x}Te_3$ thin films with exceptional flexibility for wearable energy harvesting, Carbon Energy. (2024), https://doi.org/10.1002/cey2.541 cey2.541.
[116] S. Singh, S. Jindal, S.K. Tripathi, High Seebeck coefficient in thermally evaporated Sb-In co-alloyed bismuth telluride thin film, J. Appl. Phys. 127 (5) (2020) 055103, https://doi.org/10.1063/1.5127108.
[117] Y. Mao, Y.G. Yan, K.P. Wu, H.Y. Xie, Z.K. Xiu, J.H. Yang, Q.J. Zhang, C. Uher, X.F. Tang, Non-equilibrium synthesis and characterization of n-type $Bi_2Te_{2.7}Se_{0.3}$ thermoelectric material prepared by rapid laser melting and solidification, RSC Adv. 7 (35) (2017) 21439–21445, https://doi.org/10.1039/c7ra02677c.
[118] F. Chen, R.H. Liu, Z. Yao, Y.F. Xing, S.Q. Bai, L.D. Chen, Scanning laser melting for rapid and massive fabrication of filled skutterudites with high thermoelectric performance, J. Mater. Chem. A 6 (16) (2018) 6772–6779, https://doi.org/10.1039/C8TA01504J.
[119] Y. Tian, I. Florenciano, H.Y. Xia, Q.Y. Li, H.E. Baysal, D.M. Zhu, E. Ramunni, S. Meyers, T.Y. Yu, K. Baert, T. Hauffman, S. Nider, B. Goeksel, F. Molina-Lopez, Facile fabrication of flexible and high-performing thermoelectrics by direct laser printing on plastic foil, Adv. Mater. (2023) 2307945, https://doi.org/10.1002/adma.202307945.
[120] J. Na, Y. Kim, T. Park, C. Park, E. Kim, Preparation of bismuth telluride films with high thermoelectric power factor, ACS Appl. Mater. Interfaces 8 (47) (2016) 32392–32400, https://doi.org/10.1021/acsami.6b10188.
[121] H.J. Song, C.C. Liu, H.F. Zhu, F.F. Kong, B.Y. Lu, J.K. Xu, J.M. Wang, F. Zhao, Improved thermoelectric performance of free-Standing PEDOT:PSS/Bi_2Te_3 films with low thermal conductivity, J. Electron. Mater. 42 (2013) 1268–1274, https://doi.org/10.1007/s11664-013-2587-y.
[122] T. Zhang, K.W. Li, C.C. Li, S.Y. Ma, H.H. Hng, L. Wei, Mechanically durable and flexible thermoelectric films from PEDOT:PSS/PVA/$Bi_{0.5}Sb_{1.5}Te_3$ nanocomposites, Adv. Electron. Mater. 3 (4) (2017) 1600554, https://doi.org/10.1002/aelm.201600554.
[123] X.L. Shi, X. Ai, Q.X. Zhang, X.F. Lu, S.J. Gu, L. Su, L.J. Wang, W. Jiang, Enhanced thermoelectric properties of hydrothermally synthesized n-type Se&Lu-codoped Bi_2Te_3, J. Adv. Ceram. 9 (2020) 424–431, https://doi.org/10.1007/s40145-020-0382-9.
[124] X.D. Zhang, J. Chen, H. Zhang, P.F. Zhu, R. Wang, F. Li, B. Li, Enhanced thermoelectric performance of 3D-printed Bi_2Te_3-based materials via adding Te/Se, J. Adv. Ceram. 9 (2) (2023) 328–337, https://doi.org/10.1016/j.jmat.2022.10.002.
[125] X. Chen, L. Feng, P. Yu, C. Liu, J. Lan, Y. Lin, X. Yang, Flexible thermoelectric films based on Bi_2Te_3 nanosheets and carbon nanotube network with high n-type performance, ACS Appl. Mater. Interfaces 13 (4) (2021) 5451–5459, https://doi.org/10.1021/acsami.0c21396.
[126] Z. Mao, Z. Wang, T. Shi, P. Zong, J. Liang, Z. Liu, P. Zhang, Y. Huang, Y. Han, K. Ahmad, Z. Almutairi, C. Wan, Sandwiched graphene/Bi_2Te_3/graphene thermoelectric film with exceptional figure ofmerit for flexibility, Adv. Mater. Interfac. 9 (17) (2022) 200555, https://doi.org/10.1002/admi.202200555.
[127] X. Zhao, C. Zhao, Y. Jiang, X. Ji, F. Kong, T. Lin, H. Shao, W. Han, Flexible cellulose nanofiber/Bi_2Te_3 composite film for wearable thermoelectric devices, J. Power Sources 479 (15) (2020) 229044, https://doi.org/10.1016/j.jpowsour.2020.229044.
[128] Y.M. Cho, K.T. Kim, G.S. Lee, S.H. Kim, The role of edge-oxidized graphene to improve the thermopower of p-type bismuth telluride-based thick films, Appl. Surf. Sci. 476 (15) (2019) 533–538, https://doi.org/10.1016/j.apsusc.2019.01.026.
[129] T. Varghese, C. Hollar, J. Richardson, N. Kempf, C. Han, P. Gamarachchi, D. Estrada, R.J. Mehta, Y. Zhang, High-performance and flexible thermoelectric films by screen printing solution-processed nanoplate crystals, Sci. Rep. 6 (2016) 33135, https://doi.org/10.1038/srep33135.
[130] L. Wang, Z. Zhang, Y. Liu, B. Wang, L. Fang, J. Qiu, K. Zhang, S. Wang, Exceptional thermoelectric properties of flexible organic-inorganic hybrids with monodispersed and periodic nanophase, Nat. Commun. 9 (2018) 3817, https://doi.org/10.1038/s41467-018-06251-9.
[131] T. Gao, B. Wang, B. Ding, J. Lee, P.W. Leu, Uniform and ordered copper nanomeshes by microsphere lithography for transparent electrodes, Nano Lett. 14 (4) (2014) 2105–2110, https://doi.org/10.1021/nl5003075.
[132] C. Chen, W. Lee, Y. Chen, C. Lu, H. Lin, C. Wu, Enhancing optical out-coupling of organic light-emitting devices with nanostructured composite electrodes consisting of indium tin oxide nanomesh and conducting polymer, Adv. Mater. 27 (33) (2015) 4883–4888, https://doi.org/10.1002/adma.201502516.
[133] P. Gao, J. He, S. Zhou, X. Yang, S. Li, J. Sheng, D. Wang, T. Yu, J. Ye, Y. Cui, Large-area nanosphere self-assembly by a micro-propulsive injection method for high throughput periodic surface nanotexturing, Nano Lett. 15 (7) (2015) 4591–4598, https://doi.org/10.1021/acs.nanolett.5b01202.
[134] L. Zhang, X. Zhong, E. Pavlica, S. Li, A. Klekachev, G. Bratina, T.W. Ebbesen, E. Orgiu, P. Samori, A nanomesh scaffold for supramolecular nanowire optoelectronic devices, Nat. Nanotechnol. 11 (2016) 900–906, https://doi.org/10.1038/NNANO.2016.125.
[135] L. Zhang, E. Pavlica, X. Zhong, F. Liscio, S. Li, G. Bratina, E. Orgiu, P. Samori, Fast-response photonic device based on oganic-crystal heterojunctions assembled into a vertical-yet-open asymmetric architecture, Adv. Mater. 29 (11) (2017) 1605760, https://doi.org/10.1002/adma.201605760.
[136] T.F. Shi, M. Chen, Z. Liu, Q. Song, Y. Ou, H. Wang, J. Liang, Q. Zhang, Z. Mao, Z. Wang, J. Zheng, Q. Han, K.M. Razeeb, P. Zong, A Bi_2Te_3-filled nickel foam

film with exceptional flexibility and thermoelectric performance, Nanomaterials 12 (10) (2022) 1693, https://doi.org/10.3390/nano12101693.
[137] T.F. Shi, M.R. Chen, C.R. Zhang, Z.D. Mao, J. Liang, Z.G. Liu, J. Zhang, Q.H. Zhang, L. Pan, Y.F. Wang, C.L. Wan, P.A. Zong, Modifying carbon fiber fabric for flexible thermoelectric energy conversion, Appl. Surf. Sci. 610 (2022) 155479, https://doi.org/10.1016/j.apsusc.2022.155479.
[138] X.B. Zhao, S.H. Hu, M.J. Zhao, T.J. Zhu, Thermoelectric properties of $Bi_{0.5}Sb_{1.5}Te_3$/polyaniline hybrids prepared by mechanical blending, Mater. Lett. 52 (3) (2002) 147–149, https://doi.org/10.1016/S0167-577X(01)00381-0.
[139] J.J. Zhu, W.L. Feng, M.R. Chen, P.A. Zong, Permeable carbon fiber based thermoelectric film with exceptional EMI shielding performance and sensor capabilities, J. Adv. Ceram. (2024) 9220922, https://doi.org/10.26599/JAC.2024.9220922.Y.
[140] N. Somdock, S. Kianwimol, A. Harnwunggmoung, A. Sakulkalavek, R. Sakdanuphab, Simultaneous stoichiometric composition and highly (00l) orientation of flexible Bi_2Te_3 thin films via optimising the DC magnetron sputter-deposition process, J. Alloys Compd. 773 (2019) 78–85, https://doi.org/10.1016/j.jallcom.2018.09.216.
[141] N.L. Kuang, Z.X. Zuo, W. Wang, R.H. Liu, Z.Y. Zhao, Optimized thermoelectric properties and geometry parameters of annular thin-film thermoelectric generators using n-type $Bi_2Te_{2.7}Se_{0.3}$ and p-type $Bi_{0.5}Sb_{1.5}Te_3$ thin films for energy harvesting, Sens. Actuator A Phys. 332 (1) (2021) 113030, https://doi.org/10.1016/j.sna.2021.113030.
[142] Z.H. Zheng, D. Yang, P.C. Zhang, F. Li, Y.X. Chen, G.X. Liang, P. Fan, Enhaneement of the thermoeleetric properties of Bi_2Te_3 nanoerystal thin films by rapid annealing, Mater. Lett. 275 (2020) 128143, https://doi.org/10.1016/j.matlet.2020.128143.
[143] N.T. Hung, A.R.T. Nugraha, E.H. Hasdeo, M.S. Dresselhaus, R. Saito, Diameter dependence of thermoelectric power of semiconducting carbon nanotubes, Phys. Rev. B 92 (16) (2015) 165426, https://doi.org/10.1103/PhysRevB.92.165426.
[144] J.P. Small, L. Shi, P. Kim, Mesoscopic thermal and thermoelectric measurements of individual carbon nanotubes, Solid State Commun. 127 (2) (2003) 181–186, https://doi.org/10.1016/S0038-1098(03)00341-7.
[145] B.A. Macleod, N.J. Stanton, I.E. Gould, D. Wesenberg, R. Ihly, Z.R. Owczarczyk, K.E. Hurst, C.S. Fewox, C.N. Folmar, K.H. Hughes, B.L. Zink, J.L. Blackburn, A.J. Ferguson, Large n- and p-type thermoelectric power factors from doped semiconducting single-walled carbon nanotube thin films, Energy Environ. Sci. 10 (10) (2017) 21682179, https://doi.org/10.1039/c7ee01130j.
[146] G.D. Zhan, J.D. Kuntz, A.K. Mukherjee, P. Zhu, K. Koumoto, Thermoelectric properties of carbon nanotube/ceramic nanocomposites, Scripta Mater. 54 (1) (2006) 77–82, https://doi.org/10.1016/j.scriptamat.2005.09.003.
[147] K.S. Novoselov, A.K. Geim, S.V. Morozov, D. Jiang, Y. Zhang, S.V. Dubonos, I.V. Grigorieva, A.A. Firsov, Electric field effect in atomically thin carbon films, Science 306 (5696) (2004) 666–669, https://doi.org/10.1126/science.1102896.
[148] M. Ishigami, J.H. Chen, W.G. Cullen, M.S. Fuhrer, E.D. Williams, Atomic structure of graphene on SiO_2, Nano Lett. 7 (6) (2007) 1643–1648, https://doi.org/10.1021/nl070613a.
[149] A.K. Geim, K.S. Novoselov, The rise of graphene, Nat. Mater. 6 (2007) 183–191, https://doi.org/10.1038/nmat1849.
[150] Y. Zhu, S. Murali, W. Cai, X. Li, J. Suk, J. Potts, Graphene and graphene oxide: synthesis, properties, and applications, Adv. Mater. 22 (35) (2010) 3906–3924, https://doi.org/10.1002/adma.201001068.
[151] K.S. Novoselov, A.K. Geim, S.V. Morozov, D. Jiang, M.I. Katsnelson, I.V. Grigorieva, S.V. Dubonos, A.A. Firsov, Two-dimensional gas of massless Dirac fermions in graphene, Nature 438 (2005) 197–200, https://doi.org/10.1038/nature04233.
[152] J.H. Chen, C. Jang, S.D. Xiao, M. Ishigami, M. Fuhrer, Intrinsic and extrinsic performance limits of graphene devices on SiO_2, Nat. Nanotechnol. 3 (2008) 206e209, https://doi.org/10.1038/nnano.2008.58.
[153] P.A. Zong, J. Liang, P. Zhang, C.L. Wan, Y.F. Wang, K. Koumoto, Graphene-based thermoelectrics, ACS Appl. Energy Mater. 3 (3) (2020) 2224–2239, https://doi.org/10.1021/acsaem.9b02187.
[154] Y.C. Zhang, Q.C. Zhang, G.M. Chen, Carbon and carbon composites for thermoelectric applications, Carbon Energy. 2 (3) (2020) 408–436, https://doi.org/10.1002/cey2.68.
[155] Y.J. Huang, C.L. Wan, Controllable fabrication and multifunctional applications of graphene/ceramic composites, J. Adv. Ceram. 9 (2020) 271–291, https://doi.org/10.1007/s40145-020-0376-7.
[156] S. Park, J.H. An, I.W. Jung, R.D. Piner, S.J. An, X.S. Li, A. Velamakanni, R.S. Ruoff, Colloidal suspensions of highly reduced graphene oxide in a wide variety of organic solvents, Nano Lett. 9 (4) (2009) 1593–1597, https://doi.org/10.1021/nl803798y.
[157] C. Lee, X.D. Wei, J.W. Kysar, J. Hone, Measurement of the elastic properties and intrinsic strength of monolayer graphene, Science 321 (5887) (2008) 385–388, https://doi.org/10.1126/science.1157996.
[158] B. Wu, Y. Guo, C.Y. Hou, Q.H. Zhang, Y.G. Li, H.Z. Wang, High-performance flexible thermoelectric devices based on all-inorganic hybrid films for harvesting low-grade heat, Adv. Funct. Mater. 29 (25) (2019) 1900304, https://doi.org/10.1002/adfm.201900304.
[159] D.F. Ding, F.M. Sun, F. Xia, Z.Y. Tang, A high-performance and flexible thermoelectric generator based on the solution-processed composites of reduced graphene oxide nanosheets and bismuth telluride nanoplates, Nanoscale Adv. 2 (8) (2020) 3244–3251, https://doi.org/10.1039/d0na00118j.
[160] S.H. Jung, K.T. Kim, G.S. Lee, J.Y. Sun, D.W. Kim, Y.S. Yom, D.Y. Yang, J. Yu, J.M. Park, D.Y. Hyeon, K.I. Park, Synergistically improved thermoelectric energy harvesting of edge-oxidized-graphene-bridged n-type bismuth telluride thick films, ACS Appl. Mater. Interfaces 13 (4) (2021) 5125–5132, https://doi.org/10.1021/acsami.0c20509.
[161] M. Bharti, A. Singh, S. Samanta, D.K. Aswal, Conductive polymers for thermoelectric power generation, Prog. Mater. Sci. 93 (2018) 270–310, https://doi.org/10.1016/j.pmatsci.2017.09.004.
[162] G.H. Kim, L. Shao, K. Zhang, K.P. Pipe, Engineered doping of organic semiconductors for enhanced thermoelectric efficiency, Nat. Mater. 12 (2013) 71–723, https://doi.org/10.1038/NMAT3635.
[163] K.C. See, J.P. Feser, C.E. Chen, A. Majumdar, J.J. Urban, R.A. Segalman, Water-processable polymer–nanocrystal hybrids for thermoelectrics, Nano Lett. 10 (11) (2010) 4664–4667, https://doi.org/10.1021/nl102880k.
[164] B. Zhang, J. Sun, H.E. Katz, F. Fang, R.L. Opila, Promising thermoelectric properties of commercial PEDOT:PSS materials and their Bi_2Te_3 powder-composites, ACS Appl. Mater. Interfaces 2 (11) (2010) 3170–3178, https://doi.org/10.1021/am100654p.
[165] Y. Wang, Research progress on a novel conductive polymer–poly(3,4-ethylenedioxythiophene) (PEDOT), J. Phys. Conf. Ser. 152 (2009) 012023, https://doi.org/10.1088/1742-6596/152/1/012023.
[166] S. Dutta, J. Kim, Y. Ide, J.H. Kim, M.S.A. Hossain, Y. Bando, Y. Yamauchi, K.C.W. Wu, 3D network of cellulose-based energy storage devices and related emerging applications, Mater. Horiz. 4 (4) (2017) 522–545, https://doi.org/10.1039/C6MH00500D.
[167] Y. Chen, S.Y. Chen, B.X. Wang, J.J. Yao, H.P. Wang, TEMPO-oxidized bacterial cellulose nanofibers-supported gold nanoparticles with superior catalytic properties, Carbohydr. Polym. 160 (15) (2017) 34–42, https://doi.org/10.1016/j.carbpol.2016.12.020.
[168] Z.Q. Fang, G.Y. Hou, C.J. Chen, L.B. Hu, Nanocellulose-based films and their emerging applications, Curr. Opin. Solid State Mater. Sci. 23 (4) (2019) 100764, https://doi.org/10.1016/j.cossms.2019.07.003.
[169] J.H. Kim, D.G. Lee, Y.H. Lee, W.S. Chen, S.Y. Lee, Nanocellulose for energy storage systems: beyond the limits of synthetic materials, Adv. Mater. 31 (20) (2018) 1804826, https://doi.org/10.1002/adma.201804826.
[170] K. Bethke, S. Palantöken, V. Andrei, M. RoSS, V.S. Raghuwanshi, F. Kettemann, K. Greis, T.T.K. Ingber, J.B. Stuckrath, S. Valiyaveettil, K. Rademann, Functionalized cellulose for water purification, antimicrobial applications, and sensors, Adv. Funct. Mater. 28 (23) (2018) 1800409, https://doi.org/10.1002/adfm.201800409.
[171] H. Oh, S.S. Kwak, B. Kim, E. Han, G.H. Lim, S.W. Kim, B. Lim, Highly conductive ferroelectric cellulose composite papers for efficient triboelectric nanogenerators, Adv. Funct. Mater. 29 (37) (2019) 1904066, https://doi.org/10.1002/adfm.201904066.
[172] S. M/Kulikov, V.P. Plekhanov, A.I. Tsyganok, C. Schlimm, E. Heitz, Electrochemical reductive dechlorination of chlororganic compounds on carbon cloth and metal-modified carbon cloth cathodes, Electrochim. Acta 41 (4) (1996) 527–531, https://doi.org/10.1016/0013-4686(95)00339-8.
[173] T. Kang, J. Kim, Optimal cobalt-based catalyst containing high-ratio of oxygen vacancy synthesized from metal-organic-framework (MOF) for oxygen evolution reaction (OER) enhancement, Appl. Surf. Sci. 560 (2021) 150035, https://doi.org/10.1016/j.apsusc.2021.150035.
[174] X.D. Ma, J.Y. Xia, X.H. Wu, Z.Y. Pan, P.K. Shen, Remarkable enhancement in the electrochemical activity of maricite $NaFePO_4$ on high-surface-area carbon cloth for sodium-ion batteries, Carbon 146 (2019) 78–87, https://doi.org/10.1016/j.carbon.2019.02.004.
[175] X.P. He, B. Gao, G.B. Wang, J.T. Wei, C. Zhao, A new nanocomposite: carbon cloth based polyaniline for an electrochemical supercapacitor, Electrochim. Acta 111 (30) (2013) 210–215, https://doi.org/10.1016/j.electacta.2013.07.226.
[176] M. Kim, D. Park, J. Kim, A thermoelectric generator comprising selenium-doped bismuth telluride on flexible carbon cloth with n-type thermoelectric properties, Ceram. Int. 48 (8) (2022) 10852–10861, https://doi.org/10.1016/j.ceramint.2021.12.302.
[177] Y. Li, Y. Zhao, J. Qiao, S. Jiang, J. Qiu, J. Tan, L. Zhang, Z. Gai, K. Tai, C. Liu, A flexible and infrared-transparent Bi_2Te_3-Carbon nanotube thermoelectric hybrid for both active and passive cooling, ACS Appl. Electron. Mater. 2 (9) (2020) 3008–3016, https://doi.org/10.1021/acsaelm.0c00617.
[178] J.Z. Rogers, T. Someya, Y.G. Huang, Materials and mechanics for stretchable electronics, Science 327 (5973) (2010) 1603–1607, https://doi.org/10.1126/science.1182383.
[179] H. Hosono, How we made the IGZO transistor, Nat. Electron. 1 (7) (2018) 428, https://doi.org/10.1038/s41928-018-0106-0, 428.
[180] C.L. Wan, X.K. Gu, F. Dang, T. Itoh, Y.F. Wang, H. Sasaki, M. Kondo, K. Koga, K. Yabuki, G.J. Snyder, R.G. Yang, K. Koumoto, Flexible n-type thermoelectric materials by organic intercalation of layered transition metal dichalcogenide TiS_2, Nat. Mater. 14 (6) (2015) 622–627, https://doi.org/10.1038/NMAT4251.
[181] J. Peng, G.J. Snyder, A figure of merit for flexibility, Science 366 (6466) (2019) 690691, https://doi.org/10.1126/science.aaz5704.
[182] B. Hamdou, J. Kimling, A. Dorn, E. Pippel, R. Rostek, P. Woias, K. Nielsch, Thermoelectric characterization of bismuth telluride nanowires, synthesized via catalytic growth and post-annealing, Adv. Mater. 25 (2) (2012) 239–244, https://doi.org/10.1002/adma.201202474.

[183] R. Rostek, V. Sklyarenko, P. Woias, Influence of vapor annealing on the thermoelectric properties of electrodeposited Bi_2Te_3, J. Mater. Res. 26 (2011) 1785–1790, https://doi.org/10.1557/jmr.2011.141.
[184] Y.C. Li, S.L. Bai, Y. Wen, Z. Zhao, L. Wang, S.B. Liu, J.Q. Zheng, S.Q. Wang, S. Liu, D.Z. Gao, D.R. Liu, Y.C. Zhu, Q. Cao, X. Gao, H.Y. Xie, L.D. Zhao, Realizing high-efficiency thermoelectric module by suppressing donor-like effect and improving preferred orientation in n-type $Bi_2(Te, Se)_3$, Sci. Bull. (2024) 04034, https://doi.org/10.1016/j.scib.2024.04.034.
[185] Z.J. Chen, H.C. Lv, Q.C. Zhang, H.F. Wang, G.M. Chen, Construction of a cement–rebar nanoarchitecture for a solution-processed and flexible film of a Bi_2Te_3/CNT hybrid toward low thermal conductivity and high thermoelectric performance, Carbon Energy. 4 (1) (2021) 115–128, https://doi.org/10.1002/cey2.161.
[186] T. Chiba, H. Yabuki, M. Takashiri, High thermoelectric performance of flexible nanocomposite films based on Bi_2Te_3 nanoplates and carbon nanotubes selected using ultracentrifugation, Sci. Rep. 13 (1) (2023) 3010, https://doi.org/10.1038/s41598-023-30175-0.
[187] Y. Kawajiri, S.A. Tanusilp, M. Kumagai, M. Ishimaru, Y. Ohishi, J. Tanaka, K. Kurosaki, Enhancement of thermoelectric properties of n-type $Bi_2Te_{3-x}Se_x$ by energy filtering effect, ACS Appl. Energy Mater. 4 (10) (2021) 11819–11826, https://doi.org/10.1021/acsaem.1c02560.
[188] C. Gayner, Y. Amouyal, Energy filtering of charge carriers: current trends, challenges, and prospects for thermoelectric materials, Adv. Funct. Mater. 30 (18) (2020) 1901789, https://doi.org/10.1002/adfm.201901789.
[189] K. Agarwal, V. Kaushik, D. Varandani, A. Dhar, B.R. Mehta, Nanoscale thermoelectric properties of Bi_2Te_3-Graphene nanocomposites: conducting atomic force, scanning thermal and kelvin probe microscopy studies, J. Alloys Compd. 681 (2016) 394–401, https://doi.org/10.1016/j.jallcom.2016.04.161.
[190] C.L. Xiong, F.F. Shi, H.X. Wang, J.F. Cai, S.M. Zhao, X.J. Tan, H.Y. Hu, G.Q. Liu, J.G. Noudem, J. Jiang, Achieving high thermoelectric performance of n-Type $Bi_2Te_{2.79}Se_{0.21}$ sintered materials by hot-stacked deformation, ACS Appl. Mater. Interfaces 13 (13) (2021) 15429–15436, https://doi.org/10.1021/acsami.1c02417.
[191] Z.J. Chen, H.C. Lv, Q.C. Zhang, H.F. Wang, G.M. Chen, Construction of a cement–rebar nanoarchitecture for a solution-processed and flexible film of a Bi_2Te_3/CNT hybrid toward low thermal conductivity and high thermoelectric performance, Carbon Energy. 4 (1) (2022), https://doi.org/10.1002/cey2.161.
[192] H. Zhu, J.Y. Zhao, C. Xiao, Improved thermoelectric performance in n-type BiTe facilitated by defect engineering, Rare Met. 40 (10) (2021) 2829–2837, https://doi.org/10.1007/s12598-021-01737-w.
[193] H. An, M. Pusko, D. Chun, S. Park, J. Moon, In-situ synthesis of flexible hybrid composite films for improved thermoelectric performance, Chem. Eng. J. 357 (2018) 547–558, https://doi.org/10.1016/j.cej.2018.09.200.
[194] P.A. Zong, Z.W. Wang, C.R. Zhang, Z.G. Liu, M.R. Chen, W.H. Li, Q.C. Han, Q.H. Zhang, W.L. Feng, C.L. Wan, Boosting thermoelectric performance of $Ba_yCo_4Sb_{12}$ by interlinking large-aspect-ratio silver nanowires at the triple junction of grain boundaries, Mater. Today Energy 26 (2022) 101007, https://doi.org/10.1016/j.mtener.2022.101007.
[195] C.W. Nan, G. Liu, Y. Lin, M. Li, Interface effect on thermal conductivity of carbon nanotube composites, Appl. Phys. Lett. 85 (16) (2004) 3549–3551, https://doi.org/10.1063/1.1808874.
[196] S.T. Huxtable, D.G. Cahill, S. Shenogin, L.P. Xue, R. Ozisik, P. Barone, M. Usrey, M. Strano, G. Siddons, M. Shim, P. Keblinski, Interfacial heat flow in carbon nanotube suspensions, Nat. Mater. 2 (2003) 731–734, https://doi.org/10.1038/nmat996.
[197] K. Ahmad, C. Wan, M.A. Al-Eshaikh, A.N. Kadachi, Enhanced thermoelectric performance of Bi_2Te_3 based graphene nanocomposites, Appl. Surf. Sci. 474 (2019) 2–8, https://doi.org/10.1016/j.apsusc.2018.10.163.
[198] Y. Li, Z.P. Chen, C.Y. Gao, H.P. Li, X.H. Fan, X.B. Cao, L.M. Yang, Electrochemical assembly of flexible PPy/Bi–Te alloy/PPy thermoelectric composite films with a sandwich-type structure, New J. Chem. 48 (4) (2024) 1634–1641, https://doi.org/10.1039/D3NJ04785G.
[199] S.H. Yang, H.W. Ming, C. Zhu, Z.Y. Wang, H.X. Xin, Z.H. Ge, D. Li, J. Zhang, X.Y. Qin, High Thermoelectric performance of n-type BiTeSe-based composites incorporated with both inorganic and organic nanoinclusions, ACS Appl. Mater. Interfaces 16 (13) (2024) 16732–16743, https://doi.org/10.1021/acsami.4c02032.
[200] W. Thongkham, C. Lertsatitthanakorn, K. Jiramitmongkon, K. Tantisantisom, T. Boonkoom, M. Jitpukdee, K. Sinthiptharakoon, A. Klamchuen, M. Liangruksa, P. Khanchaitit, Self-assembled three-dimensional Bi_2Te_3 nanowire–PEDOT:PSS hybrid nanofilm network for ubiquitous thermoelectrics, ACS Appl. Mater. Interfaces 11 (6) (2019) 6624–6633, https://doi.org/10.1021/acsami.8b19767.
[201] P.A. Zong, P. Zhang, S.J. Yin, Y.J. Huang, Y.L. Wang, C.L. Wan, Fabrication and characterization of a cybrid Bi_2Se_3/Organic superlattice for thermoelectric energy conversion, Adv. Electron. Mater. 5 (11) (2019) 1800842, https://doi.org/10.1002/aelm.201800842.
[202] C.J. Yao, H.L. Zhang, Q. Zhang, Recent Progress in Thermoelectric materials based on conjugated polymers, Polymers 11 (1) (2019) 107, https://doi.org/10.3390/polym11010107.